PCCP

PAPER

View Article Online
View Journal | View Issue

Cite this: *Phys. Chem. Chem. Phys.*, 2025, **27**, 23765

Electronic structure and chemical bonding of the MoBe molecule

Constantinos Demetriou[a] and Demeter Tzeli *[ab]

Molybdenum beryllium materials are being researched and applied in cutting-edge technologies. It has been found that beryllium, even though it has a full 2s subshell, can form a variety of bonds with specific atoms. Here, the simple building block, the MoBe molecule, is investigated to shed light in their bonding. Specifically, forty-three low-lying states of MoBe have been investigated *via* complete active space self-consistent field (CASSCF) and multi-reference configuration interaction (MRCISD(+Q)) using the aug-cc-pV5Z(-PP) basis set. Dissociation energies (D_e), dipole moments, and various spectroscopic constants are calculated, while potential energy curves are plotted. A variety of bonding is formed in MoBe, *i.e.*, half bonds up to the formation of triple bonds, while in most cases, Be atoms are excited at the Be(^{3}P) state. The ground state, $X^7\Sigma^+$, is well separated from the excited ones, *i.e.*, the first excited state, $a^5\Sigma^+$, is lying 15.0 kcal mol^{-1} above. The adiabatic D_e of calculated states range from 2.5 ($^9\Sigma^+(1)$, van der Waals interaction) to 57.7 kcal mol^{-1} ($b^5\Pi$). The $b^5\Pi$, $^3\Delta(1)$, and $^3\Pi(1)$ have triple bonds, while their diabatic D_e values are 86.7, 92.0 and 88.0 kcal mol^{-1}. The MRCISD+Q bond distances range from 2.047 ($^3\Delta(1)$) to 2.787 Å ($^9\Sigma^+(1)$), while dipole moments range from 1.51 to 3.28 D. Overall, the present work highlights the exceptional ability of beryllium atoms to participate in a variety of bonding schemes, and it could provide the opening gate for further investigation of this species or associated materials and complexes.

Received 7th August 2025,
Accepted 15th October 2025

DOI: 10.1039/d5cp03025k

rsc.li/pccp

1 Introduction

Materials containing rare metallic elements, such as molybdenum (Mo), have been under extensive investigation and research due to the exceptional properties they present, such as high thermal and corrosion resistance, and good mechanical performance. Alloying Mo with other elements can further enhance these properties, making it suitable for demanding applications. For example, this element is used in high-temperature environments, such as in aerospace and nuclear technology, *i.e.* rocket nozzles and components in nuclear reactors.[1–4] Furthermore, it is employed in applications that require improved strength and is suitable for situations demanding high mechanical performance.[5,6] Incidentally, molybdenum beryllium materials, containing Mo–Be bonds, are being researched and applied across these industries, due to the unique physical and chemical properties of both elements,[7–11] as well as they have been implemented in surface science, where they are being studied especially for their reflective properties as coated mirrors.[12–14] Despite this, the molecular and electronic structure of the ground and excited states of the molybdenum beryllium diatomic molecule have not been investigated, while their bonding has not been explored.

It has been extensively stressed that the elucidation of such bonding schemes inside the simplest building blocks of such compounds, which are their diatomic molecules, contributes greatly to the understanding of the bonding arising inside more complex systems comprised of them.[15] While this feature is bountiful, their accurate description on a theoretical level poses a demanding task, due to their computational complexity rising from their high density of states and the high space-spin angular momentum of the contained transition metal atoms. Therefore, the understanding of the bonding schemes between a transition metal element and a main group element is not an easy task.[16] A thorough inspection into the simplest building blocks of such compounds is the steppingstone towards the investigation of more complex systems. For instance, in the case of the MoS_2 2D material, it was found that the low-lying septet states of the diatomic MoS[17] and triatomic MoS_2 molecules are involved in the material as a building block, explaining the variety of its morphologies.[18]

Efforts in the exploration of the electronic structure of molybdenum compounds are constantly ongoing, owing to the key role they present in molecular biology, namely in

[a] *Laboratory of Physical Chemistry, Department of Chemistry, National and Kapodistrian University of Athens, Athens, Greece. E-mail: tzeli@chem.uoa.gr*
[b] *Theoretical and Physical Chemistry Institute, National Hellenic Research Foundation, Athens, Greece*

nitrogen fixation and oxidation catalysis.[19,20] Incidentally, molybdenum (Mo) presents quite a unique electronic configuration as an element, that is, all of its valence subshells are half filled; Mo: [Kr] $4d^5 5s^1$, which in turn provides it with a bonding profile that allows it to participate in a multitude of bonding schemes, with some of them resulting in significant properties in the forming compounds.[21–25]

Conversely, beryllium (Be) presents an electronic configuration of a completely closed and occupied valence subshell orbital; Be: [He] $2s^2$. For this reason, one would expect beryllium to be highly inert, like its brethren helium (He), but in reality, Be has been found to form many different compounds uer a lot of bonding schemes,[26–40] where beryllium forms from single bonds[26–33] to multiple bonds,[34–40] for instance delocalized bonds,[36] double,[37] triple bonds,[38] and even quadruple bonds.[39,40] Quadruple bonds are observed in the case of the PdBe molecule and $PbBe^-$ anion, specifically four datives Pd–Be bonds are formed: $(4d_{xz} \rightarrow 2p_x)^2$, $(4d_{yz} \rightarrow 2p_y)^2$, $(4d_{z^2} \rightarrow 2p_z)^2$, and $(5s_0 \leftarrow 2s)^2$ in the $X^1\Sigma^+$ state of PbBe[39] and $(4d_{xz} \rightarrow 2p_x)^2$, $(4d_{yz} \rightarrow 2p_y)^2$, $(4d_{z^2} \rightarrow 2p_z)^2$, and $(5p_z \leftarrow 2s)^2$ in the $X^2\Sigma^+$ state of the $PdBe^-$ anion.[40] The corresponding dissociation energies are 52.8 kcal mol^{-1} and 56.7 kcal mol^{-1} respectively at MRCISD+Q/aug-cc-pV5Z(-PP).[39,40] Recently, the electronic spectra for CuBe, which is isovalent with the $PdBe^-$ anion, were recorded using resonantly enhanced one-color, two-photon ionization and calculated *via* CCSD(T) and DFT methodology and it was found that the ground state, $X^2\Sigma^+$, has a dissociation energy (D_e) of 26.7 kcal mol^{-1} at RCCSD(T)+DKH2/cc-pwCVQZ-DK.[41]

Overall, most diatomic molecules of molybdenum have been studied extensively, but this does not hold for the MoBe molecule. To the best of our knowledge, there exist a complete lack of theoretical examination on the MoBe diatomic, while only recently has there been any theoretical investigation regarding it, carried out by our team, where the ground state of the MoX molecules, where X = Li, Be, B, C, O, N, F *via* multireference and coupled cluster methodologies with the inclusion of correlation energy calculations of both core ($4s^2 4p^6$ of Mo and $1s^2$ of X) + valence electrons having been carried out.[42,43] Here, we have shed light into the electronic spectrum of MoBe for the first time. Specifically, we have investigated the ground state and 42 low-lying states of the MoBe molecule *via* complete active space self-consistent field (CASSCF), while nine (9) of them were further investigated *via* multi-reference configuration interaction (MRCISD and MRCISD+Q). The present study aims to deliver a more detailed discussion of the properties of this molecule, with high precision calculations and to fill the gap in the study of the diatomic molecules. Furthermore, the selected calculated states are correlated with material or complexes where the Mo–Be bonds are included in their structure.

2 Computational details

The electronic structure of the MoBe molecule was studying using the state-average complete active space self-consistent field (SA-CASSCF),[44,45] CASSCF (without employing any state average technique),[44] and multireference configuration interaction plus single and double excitations (CASSCF + single + double replacements = MRCISD)[46] methodologies. All calculations were carried out using the augmented correlation consistent polarized valence basis sets of quintuple-ζ quality, *i.e.*, Mo: aug-cc-pV5Z-PP[47] and Be: aug-cc-pV5Z.[48] For the Mo atom, the accurate core relativistic ECP28MDF pseudopotential developed from the Stuttgart/Köln group[49] has been used, which equates to 28 core electrons *i.e.*, $1s^2 2s^2 2p^6 3s^2 3p^6 3d^{10}$ electrons. Thus, the $4s^2 4p^6 4d^5 5s^1$ electrons of Mo were treated *via ab initio* calculations using the contracted basis of [8s8p7d5f4g3h2i] and $1s^2 2s^2$ electrons of Be were treated using the contracted [7s6p5d4f3g2h] basis set. Instead of using a relativistic pseudopotential on Mo (as in the present calculations), scalar relativistic effects (mass–velocity and Darwin terms) can be included *via* an all-electron basis set appropriate for the second-order Douglas–Kroll–Hess (DKH2) approach. Previous calculations from our group on the MoC molecule[21] showed that including scalar relativistic effects *via* DKH2 resulted in bond distances and dissociation energies very similar to those obtained using accurate core-relativistic pseudopotentials of the aug-cc-pV5Z-PP basis set.[21] Therefore, we expect that both methodological approaches will yield similar results for the MoBe molecule. Accordingly, in the present work we use only the approach based on basis sets with accurate relativistic pseudopotentials.

Finally, regarding the inclusion of spin–orbit coupling for the lowest states, it is found that the ground and first excited states are both Σ states, *i.e.*, $X^7\Sigma^+$ and $a^5\Sigma^+$. Their energy difference is 15.5 kcal mol^{-1} at the MRCISD level, which is a relatively large separation; thus, inclusion of spin–orbit coupling is not expected to significantly affect their relative energy ordering.

At first, 43 states were studied *via* SA-CASSCF/aug-cc-pV5Z(-PP) method.[45,47,48] The SA-CASSCF reference wavefunctions are obtained by distributing eight active electrons [Mo ($4d^5 5s^1$) + Be ($2s^2$)] to ten orbital functions, one ''5s'' and five ''4d'' orbitals on Mo, one ''2s'' and three ''2p'' orbitals on Be. All calculations were carried out under C_{2v} symmetry constraints. The CASSCF wavefunctions have the correct axial angular momentum symmetry, *i.e.*, $|\Lambda|$ = 0 (Σ^+, Σ^-), 1 (Π), 2 (Δ), 3 (Φ), 4 (Γ), 5 (H), 6 (I). Thus, Σ^+ corresponds to A_1 symmetry, Σ^- corresponds to A_2; Δ, Γ, and I are linear combinations of A_1 and A_2 symmetries, while Π, Φ, and H are linear combinations of B_1 and B_2 symmetries. The SA-CASSCF was applied for states within the same multiplicity of spin, while two groups were obtained for each multiplicity of spin, *i.e.*, the first one contains four states of the A_1 and four states of A_2 symmetries, which includes Σ^+, Σ^-, Δ, Γ, and I, and the second one contains four states of B_1 and four states of B_2 symmetries, which includes Π, Φ, and H. All states at the SA-CASSCF/aug-cc-pV5Z(-PP) method are optimized with weight 1. The thresholds used are: 10^{-5} for the orbital gradient and 10^{-8} for change of the total energy.

Then nine states out of forty-three, *i.e.*, the lowest in energy states and some selected ones were further studied *via*

CASSCF/aug-cc-pV5Z(-PP)[44,47,48] followed by the MRCISD/aug-cc-pV5Z(-PP)[46–48] method. Note that MRCISD wavefunctions may not display pure spatial angular momentum symmetry, however, in the present calculations, their CASSCF wavefunctions have the correct spatial angular momentum symmetry and thus the corresponding MRCISD wavefunctions retain the same axial angular momentum symmetry.[45]

The CASSF reference spaces consist of 5154 ($^3\Sigma^+$), 5220 ($^3\Pi$), 5196 ($^3\Delta$), 2070 ($^5\Sigma^+$), 2060 ($^5\Pi$), 303 ($^7\Sigma^+$), 292 ($^7\Pi$), 9 ($^9\Sigma^+$), and 12 ($^9\Pi$) configuration state functions (CSFs). The corresponding MRCISD spaces consist of 2×10^8 ($^3\Sigma^+$, $^3\Pi$, $^3\Delta$), 1×10^8 ($^5\Sigma^+$, $^5\Pi$), 3×10^7 ($X^7\Sigma^+$, $^7\Pi$), 2×10^6 ($^9\Sigma^+$, $^9\Pi$) CSFs. The thresholds used are: 10^{-5} for the orbital gradient and 10^{-8} for the change of the total energy. In all multireference calculations, the internal contraction scheme was used,[50] where the multireference CSFs were reduced by about two orders of magnitude. Since this scheme is used for all multireference calculations, the notation MRCISD will be used for simplicity. Finally, the Davidson correction for unlinked quadruples (+Q)[51] was employed, which minimizes the size non-extensivity problems.

For all calculated states, bond distances, dissociation energies, and other spectroscopic constants have been computed at all levels of theory. The corresponding potential energy curves (PECs) have been plotted. Additionally, for some states where avoided crossings were observed, their diabatic PECs are also plotted. Furthermore, spectroscopic constants were obtained *via* a Dunham analysis.[52] Moreover, the chemical bonding is analyzed. In each case, the bonding has been plotted *via* 2-D valence bond Lewis (vbL) diagrams and *via* the 3D plot of the valence molecular orbitals. Mulliken population analysis[53] is also included using a small correlation consistent polarized valence basis set of triple-ζ quality basis set, cc-pVTZ(-PP), since Mulliken population analysis is basis set dependent, and it provides better data with simple non-augmented basis sets.[54] It is generally accepted that population analysis, either Mulliken or natural population analysis, helps in comparing similar states of the same molecule.[54] All computations were carried out using the MOLPRO[55] code.

3 Results & discussion

3.1 SA-CASSCF

On the basis that a complete lack of any previous background, on either experimental or theoretical grounds regarding the picture on the electronic spectra of MoBe, as a starting point exploratory SA-CASSCF calculations were carried out to determine 43 electronic states and set the scene. Specifically, 10 nonet states, *i.e.* $^9(\Sigma^+$ [2], Σ^- [2], Π [3], Δ [2], Φ, $\Gamma)$, 11 septet states, *i.e.* $^7(\Sigma^+$ [3], Σ^- [2], Π [3], Δ [2], $\Phi)$, 11 quintet states, *i.e.* $^5(\Sigma^+$ [3], Σ^-, Π [3], Δ [2], Φ, $\Gamma)$, and 11 triplet states, *i.e.* $^3(\Sigma^+$ [2], Σ^-, Π [3], Δ [3], Φ, $\Gamma)$, with the numbers in the square brackets *i.e.*, Π[3], denoting that three Π states have been calculated. The calculated states are correlated to Mo(a^7S, a^5S, a^5D, a^5G, a^5P, a^3P, a^3D, a^3G) + Be(^{1}S, ^{3}P), adiabatically. It is worth noting

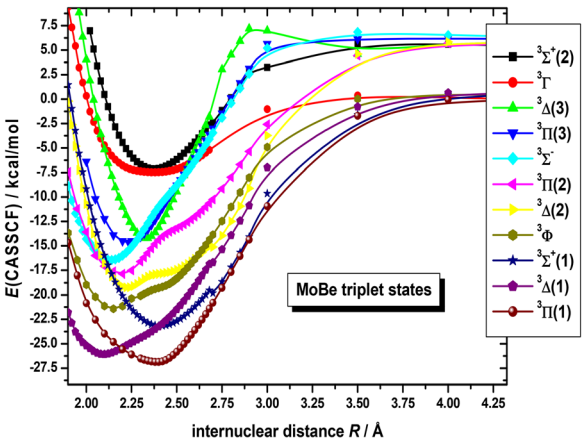

Fig. 1 Potential energy curves (PECs) of the eleven triplet states of MoBe at the SA-CASSCF/aug-cc-pV5Z(-PP) computational level. The Mo(a^3G) + Be(^{1}S) limit, to which the lowest in energy triplet states, $^3\Pi(1)$, $^3\Delta(1)$, and $^3\Sigma^+(1)$, correlate, is used to define the zero of energy.

that the triplet excited states of Mo, *i.e.*, a^3P, a^3D, and a^3G, are very close lying. Additionally, regarding which of their j term lies lowest in energy, a^3P_0 lies lower than a^3D_1, which in turn lies lower than a^3G_3, meaning that their ordering is exactly like that of a^3P, a^3D, and a^3G. However, because the calculation that were carried out considered their *j*-average term, the a^3G term will be regarded as the lowest one, and this is the reason why the triplet states of MoBe correlate adiabatically to the a^3G term.

The SA-CASSCF PECs for all calculated molecular states are plotted in Fig. 1–4, and, additionally, their bond distances as well as their relative energy differences are also provided in Table 1. Due to having retrieved a large number of calculated spin states with the same angular momentum symmetries, for clarity regarding their energetic succession we have included the ordering inside parenthesis, *i.e.*, $^5\Sigma^+(1)$ is the first $^5\Sigma^+$ state, while $^5\Sigma^+(2)$ is the second $^5\Sigma^+$ state. The bond distances range from 2.096 Å (in $^3\Delta(1)$) up to 3.459 Å (in $^9\Sigma^+(2)$). Interestingly, the shortest bond distances are observed in triplet and quintet

Table 1 Equilibrium bond distances (R_e/Å) and relative energy differences with respect to the ground electronic state, $X^7\Sigma^+$, (T_e/kcal mol^{-1}) of 43 calculated states of MoBe at the SA-CASSCF/aug-cc-pV5Z level of theory

State	R_e	T_e	State	R_e	T_e	State	R_e	T_e
$X^7\Sigma^+$	2.497	0	$^5\Gamma$	2.505	53.0	$^7\Pi(3)$	2.574	65.9
$^5\Sigma^+(1)$	2.474	11.3	$^3\Phi$	2.151	53.8	$^3\Gamma$	2.379	67.6
$^5\Pi(1)$	2.293	26.0	$^5\Sigma^-$	2.401	55.2	$^3\Sigma^+(2)$	2.375	67.9
$^7\Pi(1)$	2.438	36.3	$^7\Sigma^+(3)$	2.746	55.3	$^7\Delta(2)$	2.699	70.1
$^5\Pi(2)$	2.329	38.4	$^9\Pi(1)$a	2.556	55.4	$^7\Sigma^-(1)$	2.603	71.8
$^5\Sigma^+(2)$	2.373	39.5	$^3\Delta(2)$	2.226	55.8	$^7\Sigma^-(2)$	2.395	88.4
$^7\Sigma^+(2)$	2.521	43.1	$^3\Pi(2)$	2.179	57.1	$^9\Sigma^-(1)$	2.461	93.4
$^5\Phi$	2.321	43.6	$^3\Sigma^-$	2.136	58.6	$^9\Pi(2)$	2.889	101.6
$^5\Delta(1)$	2.419	43.8	$^7\Pi(2)$	2.569	59.9	$^9\Phi$	2.875	108.3
$^5\Sigma^+(3)$	2.485	44.4	$^3\Pi(3)$	2.234	60.4	$^9\Delta(1)$	2.979	108.3
$^5\Delta(2)$	2.456	47.2	$^3\Delta(3)$	2.339	60.8	$^9\Sigma^-(2)$	2.957	109.8
$^3\Pi(1)$	2.399	48.2	$^7\Phi$	2.569	63.3	$^9\Pi(3)$	2.903	109.8
$^3\Delta(1)$	2.096	49.0	$^9\Sigma^+(1)$	2.597	64.3	$^9\Delta(2)$	2.607	116.3
$^5\Pi(3)$	2.671	49.7	$^7\Delta(1)$	2.735	64.5	$^9\Sigma^+(2)$	3.459	122.5
$^3\Sigma^+(1)$	2.409	51.9						

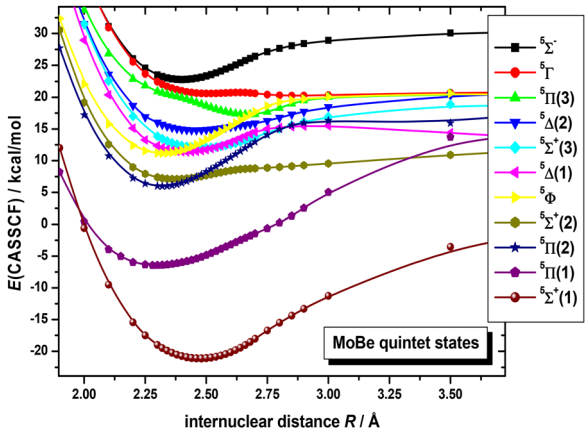

Fig. 2 Potential energy curves (PECs) of eleven quintet states of MoBe at the SA-CASSCF/aug-cc-pV5Z(-PP) computational level. The Mo(a^5S) + Be(^1S) limit, to which the $^5\Sigma^+(1)$ state correlates, is used to define the zero of energy.

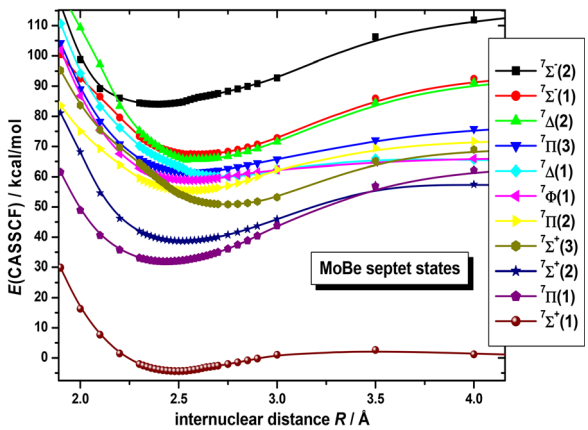

Fig. 3 Potential energy curves (PECs) of eleven septet states of MoBe at the SA-CASSCF/aug-cc-pV5Z(-PP) computational level. The Mo(a^7S) + Be(^1S) limit, to which the $X^7\Sigma^+(1)$ state correlates, is used to define the zero of energy.

states, *i.e.*, $^3\Delta(1)$, $^3\Sigma^-(1)$, $^3\Phi(1)$, $^3\Pi(2)$, $^3\Delta(2)$, $^3\Pi(3)$, $^5\Pi(1)$, see Table 1, which, at the MRCISD/aug-cc-pV5Z level of theory, showcase identical bonding schemes, see discussion bellow.

The PECs of the triplet states of MoBe are plotted in Fig. 1. They are lying about 48 kcal mol^{-1} ($\approx$1.7 eV) above the ground state and they present bond distances around 2.1–2.2 Å, see Table 1. As seen in Fig. 1, at around 2.3 Å, an avoided crossing between the $^3\Pi(2)$ with the $^3\Pi(3)$ state occurs, where the corresponding states interexchange configurations. Similarly, the $^3\Delta(1)$ state appears to be coupled to the $^3\Delta(2)$ state, where an avoided crossing occurs at around 2.3 Å. Additionally, the $^3\Delta(2)$ state presents a coupling to the $^3\Delta(3)$ state, where an avoided crossing occurs at around 2.3 Å, too. Furthermore, the $^3\Delta(3)$ state presents, another coupling to some higher in energy state, that has not been calculated, however their crossing is easily observed in their configurations, as depicted in Fig. 1, at around 2.9 Å. Lastly, the $^3\Phi(1)$, and $^3\Sigma^-(1)$ states showcase

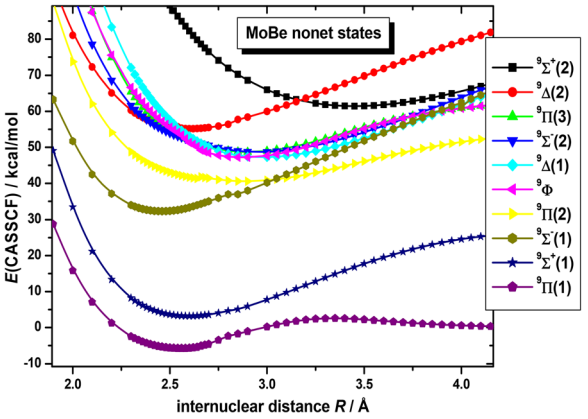

Fig. 4 Potential energy curves (PECs) of ten nonet states of MoBe at the SA-CASSCF/aug-cc-pV5Z(-PP) computational level. The Mo(a^7S) + Be(^3P) limit, to which the $^9\Pi(1)$ state correlates, is used to define the zero of energy.

avoided crossing with some higher states, cooccurring at around 2.4 Å.

Quintet states are lying about 10 kcal mol^{-1} ($\approx$0.4 eV) above the ground state, placing them adjacent to it, in reality intermediating between the ground and the rest of the septet states. Their PECs are plotted in Fig. 2, where an observant reader can discern an avoided crossing between the $^5\Pi(1)$ with the $^5\Pi(2)$ state, at around 2.5 Å, and another one, between the $^5\Pi(2)$ with the $^5\Pi(3)$ state, at around 2.75 Å, as well as between the $^5\Delta(1)$ with the $^5\Delta(2)$ state, at around 2.75 Å, as well. While not easily noticed in the quintet PECs, the $^5\Sigma^+(2)$ couples with the $^5\Sigma^+(3)$, as well, at around 2.6 Å. This was examined at the MRCISD level too, where the same avoided crossing occurs, albeit we won't be discussing it any further, as it goes beyond the scope of the present study. Lastly, the $^5\Phi(1)$, and $^5\Gamma(1)$ states showcase avoided crossing with some higher states, at around 2.5 Å, and 2.6 Å, respectively.

In Fig. 3 we have collected the eleven lowest in energy septet states. It is observed that the $X^7\Sigma^+(1)$ state, standing well separated from the bunch of the rest of the septet states., *i.e.*, it lies about 36 kcal mol^{-1} ($\approx$1.6 eV) below them, and thus it is undoubtedly the ground state of MoBe. An avoided crossing is observed between $^7\Delta(1)$ and $^7\Delta(2)$ at about 2.5 Å and they interchange their character, see Fig. 3.

Finally, the nonet states are plotted in Fig. 4, lying at about 55 kcal mol^{-1} ($\approx$2.4 eV) above the ground state. While SA-CASSCF calculations predict that the $^9\Pi(1)$ and $^9\Sigma^+(1)$ correlate to entirely different adiabatic products at their atomic limits, in the CASSCF, MRCISD, and MRCISD+Q calculations, that proceeded, it was revealed that they corelate to the exact same products, (a^7S) + Be(^3P). Moreover, while at the SA-CASSCF/aug-cc-pV5Z computational level, the PECs of $^9\Pi(1)$ and $^9\Pi(2)$ give the impression of a coupling being involved between the states, even though they are clearly separated, at the CASSCF, MRCISD, and MRCISD+Q/aug-cc-pV5Z(-PP) levels it's demonstrated that such coupling doesn't occur, and no avoided crossing between those two states takes place, as $^9\Pi(1)$ is found to be a single-reference state.

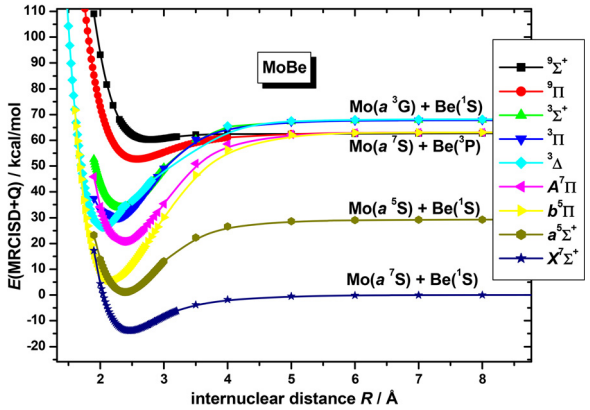

Fig. 5 PECs of the selected states of MoBe at the MRCISD+Q/aug-cc-pV5Z(-PP) computational level. The Mo(a^7S) + Be(^{1}S) limit, to which the $X^7\Sigma^+$ state correlates, is used to define the zero of energy.

3.2 MRCISD(+Q) methods

The four low-lying electronic states, $^7\Sigma^+(1)$, $^5\Sigma^+(1)$, $^5\Pi(1)$, and $^7\Pi(1)$, as well as the bunch of the three lowest lying triplet states, *i.e.* $^3\Delta(1)$, $^3\Pi(1)$, $^3\Sigma^+(1)$, which are closely packed together, along with the two lowest nonet states, $^9\Pi(1)$, and $^9\Sigma^+(1)$, were further investigated at the MRCISD(+Q) level of theory. Their PECs were calculated, see Fig. 5, while their bonding across their PECs were analyzed. It should be mentioned, as it will matter later on, that, while the $^3\Delta(1)$ lies higher in energy than the $^3\Pi(1)$ state at the SA-CASSCF and CASSCF levels of theory, at the MRCISD(+Q) computational levels the successive order of this pair is reversed, see Tables 1 and 2. Moreover, it should be noted that CASSCF and SA-CASSCF present in general the same relative energy ordering of the states, with the one exception being the high spin state $^9\Sigma^+(1)$. Additionally, the ground molecular state of MoBe, $^7\Sigma^+(1)$, along with the three lowest-lying excited states, them being $^5\Sigma^+(1)$, $^5\Pi(1)$, and $^7\Pi(1)$, are clearly separated for the remaining excited states across all used methods and their ordering is retained in all methods.

To sum up, our best results are obtained at the MRCISD+Q level; the states are named based on their MRCISD+Q energies as $X^7\Sigma^+$, $a^5\Sigma^+$, $b^5\Pi$, $A^7\Pi$, $^3\Delta(1)$, $^3\Pi(1)$, $^3\Sigma^+(1)$, $^9\Pi(1)$, and $^9\Sigma^+(1)$.

Table 2 Bond distances (R_e/Å), adiabatic dissociation energies (D_e/kcal mol^{-1}), harmonic frequencies (ω_e/cm^{-1}), anharmonic corrections ($\omega_e x_e$/cm^{-1}), dipole moments (μ/D) and excitation energies (T_e/kcal mol^{-1}) of nine electronic state of MoBe at CASSCF, MRCISD, MRCISD+Q/aug-cc-pV5Z(-PP) levels of theory

State	Methodology	R_e	D_e	ω_e	$\omega_e x_e$	μ_{FF}[a]	$\langle\mu\rangle$[a]	T_e
$X^7\Sigma^+$	SA-CASSCF[b]	2.497	4.39					0.0
	MRCISD	2.481	11.42	330.7	6.26	1.41	0.94	0.0
	MRCISD+Q	2.462	13.85	351.1	5.66	1.51		0.0
	RCCSD(T)[c]	2.481	13.51	340.3	8.22	1.28		0.0
	C-MRCISD+Q[d]	2.431	13.20	383.4	5.93	1.65		0.0
	C-RCCSD(T)[d]	2.452	14.44	349.4	11.63	1.24		0.0
$a^5\Sigma^+$	CASSCF	2.488	16.79 (48.84)[e]	383.5	2.16	4.07	4.07	6.1
	MRCISD	2.400	27.20 (59.25)[e]	406.8	2.22	3.02	4.13	15.5
	MRCISD+Q	2.392	28.20 (60.25)[e]	407.3	2.26	2.76		15.0
$b^5\Pi$	CASSCF	2.286	33.22 (62.23)[f]	412.5	2.71	3.39	3.39	17.6
	MRCISD	2.181	54.58 (83.59)[f]	505.8	3.26	2.60	2.61	20.4
	MRCISD+Q	2.177	57.72 (86.73)[f]	511.2	3.27	2.51		19.2
$A^7\Pi$	CASSCF	2.464	21.61	384.2	2.21	3.25	3.25	29.3
	MRCISD	2.365	38.81	435.7	2.18	1.96	2.14	36.2
	MRCISD+Q	2.359	42.32	436.9	2.32	1.77		34.6
$^3\Delta(1)$	CASSCF	2.087	27.23 (77.40)[g]	443.1	2.13	3.22	3.22	48.3
	MRCISD	2.045	40.66 (90.83)[g]	571.1	1.19	2.27	2.40	42.4
	MRCISD+Q	2.047	41.84 (92.01)[g]	576.7	3.53	2.14		40.2
$^3\Pi(1)$	CASSCF	2.317	27.12 (77.29)[g]	449.5	9.10	4.23	4.23	46.4
	MRCISD	2.264	36.86 (87.03)[g]	446.9	24.52	2.76	3.49	45.8
	MRCISD+Q	2.266	37.81 (87.98)[g]	456.0	24.32	2.31		43.9
$^3\Sigma^+(1)$	CASSCF	2.404	22.55 (55.63)[h]	445.6	4.14	3.72	3.72	50.0
	MRCISD	2.338	32.61 (65.69)[h]	459.7	9.70	2.43	2.88	50.0
	MRCISD+Q	2.333	34.12 (67.20)[h]	449.8	6.10	2.15		47.7
$^9\Pi(1)$	CASSCF	2.661	1.96	220.2	11.71	3.91	3.91	48.9
	MRCISD	2.581	8.88	273.5	5.38	2.72	2.98	66.1
	MRCISD+Q	2.579	10.43	278.5	4.54	2.41		66.5
$^9\Sigma^+(1)$	CASSCF	2.851	2.07	141.2	21.00	3.74	3.74	50.6
	MRCISD	2.752	1.77	198.9	9.00	3.36	3.67	72.7
	MRCISD+Q	2.787	2.48	203.4	8.12	3.28		74.1

[a] μ_{FF}: dipole moment *via* finite field; $\langle\mu\rangle$: dipole moment calculated as an expectation value. [b] At the CASSCF/aug-cc-pV5Z(-PP) level, the $X^7\Sigma^+$ state is nearly bound. At the SA-CASSCF/aug-cc-pV5Z(-PP) level, state-average of the $X^7\Sigma^+(1)$, $^7\Sigma^+(2)$, $^7\Sigma^+(3)$, $^7\Delta(1)$, $^7\Delta(2)$, $^7\Sigma^-(1)$, and $^7\Sigma^-(2)$ states, the $X^7\Sigma^+$ state is bound. [c] Ref. 42; RCCSD(T)/aug-cc-pV5Z(-PP), the valence electrons (8 electrons) are correlated. [d] Ref. 42; C-MRCISD+Q/aug-cc-pwCV5Z-(-PP), C-RCCSD(T)/aug-cc-pwCV5Z(-PP), where C- stands for core. All 18 electrons treated *via ab initio* calculations are correlated. [e] Adiabatic D_e with respect to Mo(a^5S; $4d^55s^1$) + Be(^{1}S); diabatic D_e with respect to Mo(a^7S; $4d^55s^1$) + Be(^{3}P) in parenthesis. [f] Adiabatic D_e with respect to Mo(a^5D; $4d^45s^2$) + Be(^{1}S); diabatic D_e with respect to Mo(a^7S; $4d^55s^1$) + Be(^{3}P) in parenthesis. [g] Adiabatic D_e with respect to Mo(a^3G) + Be(^{1}S); diabatic D_e with respect to Mo(a^5G) + Be(^{3}P) in parenthesis. [h] Adiabatic D_e with respect to Mo(a^3G) + Be(^{1}S); diabatic D_e with respect to Mo (a^5S) + Be (^{3}P) in parenthesis.

Table 3 Composition of the CASSCF molecular orbitals of nine selected calculated states of MoBe

State	Molecular orbital	Atomic orbitals
$X^7\Sigma^+$	1σ	$0.26\varphi_{4d_{z^2}}(\mathrm{Mo}) + 0.45\varphi_{5s}(\mathrm{Mo}) + 0.27\varphi_{5p_z}(\mathrm{Mo}) + 0.90\varphi_{2s}(\mathrm{Be}) - 0.15\varphi_{2p_z}(\mathrm{Be})$
	2σ	$0.67\varphi_{4d_{z^2}}(\mathrm{Mo}) - 0.72\varphi_{5s}(\mathrm{Mo}) + 0.12\varphi_{5p_z}(\mathrm{Mo}) + 0.15\varphi_{2s}(\mathrm{Be}) + 0.04\varphi_{5p_z}(\mathrm{Mo})$
	3σ	$0.63\varphi_{4d_{z^2}}(\mathrm{Mo}) + 0.53\varphi_{5s}(\mathrm{Mo}) - 0.05\varphi_{5p_z}(\mathrm{Mo}) - 0.39\varphi_{2s}(\mathrm{Be}) - 0.44\varphi_{2p_z}(\mathrm{Be})$
	$1\delta_+$	$1.00\varphi_{4d_{x^2-y^2}}(\mathrm{Mo})$
	$1\pi_x$	$0.97\varphi_{4d_{xz}}(\mathrm{Mo})$
	$1\pi_y$	$0.97\varphi_{4d_{yz}}(\mathrm{Mo})$
	$1\delta_-$	$1.00\varphi_{4d_{xy}}(\mathrm{Mo})$
$a^5\Sigma^+$	1σ	$0.40\varphi_{4d_{z^2}}(\mathrm{Mo}) + 0.66\varphi_{5s}(\mathrm{Mo}) - 0.33\varphi_{5p_z}(\mathrm{Mo}) + 0.70\varphi_{2s}(\mathrm{Be}) - 0.39\varphi_{2p_z}(\mathrm{Be})$
	2σ	$0.70\varphi_{4d_{z^2}}(\mathrm{Mo}) + 0.11\varphi_{5s}(\mathrm{Mo}) + 0.19\varphi_{5p_z}(\mathrm{Mo}) - 0.36\varphi_{2s}(\mathrm{Be}) - 0.54\varphi_{2p_z}(\mathrm{Be})$
	3σ	$-0.47\varphi_{4d_{z^2}}(\mathrm{Mo}) + 0.68\varphi_{5s}(\mathrm{Mo}) + 0.25\varphi_{5p_z}(\mathrm{Mo}) - 0.42\varphi_{2s}(\mathrm{Be}) - 0.47\varphi_{2p_z}(\mathrm{Be})$
	$1\delta_+$	$1.00\varphi_{4d_{x^2-y^2}}(\mathrm{Mo})$
	$1\pi_x$	$0.97\varphi_{4d_{xz}}(\mathrm{Mo})$
	$1\pi_y$	$0.97\varphi_{4d_{yz}}(\mathrm{Mo})$
	$1\delta_-$	$1.00\varphi_{4d_{xy}}(\mathrm{Mo})$
$b^5\Pi$	1σ	$0.28\varphi_{4d_{z^2}}(\mathrm{Mo}) + 0.58\varphi_{5s}(\mathrm{Mo}) + 0.30\varphi_{5p_z}(\mathrm{Mo}) + 0.87\varphi_{2s}(\mathrm{Be}) - 0.18\varphi_{2p_z}(\mathrm{Be})$
	2σ	$0.89\varphi_{4d_{z^2}}(\mathrm{Mo}) - 0.38\varphi_{5s}(\mathrm{Mo}) - 0.23\varphi_{2p_z}(\mathrm{Be})$
	$1\delta_+$	$1.00\varphi_{4d_{x^2-y^2}}(\mathrm{Mo})$
	$1\pi_x$	$0.86\varphi_{4d_{xz}}(\mathrm{Mo}) + 0.41\varphi_{2p_x}(\mathrm{Be})$
	$1\pi_y$	$0.86\varphi_{4d_{yz}}(\mathrm{Mo}) + 0.41\varphi_{2p_y}(\mathrm{Be})$
	$1\delta_-$	$1.00\varphi_{4d_{xy}}(\mathrm{Mo})$
$A^7\Pi$	1σ	$0.25\varphi_{4d_{z^2}}(\mathrm{Mo}) + 0.52\varphi_{5s}(\mathrm{Mo}) + 0.33\varphi_{5p_z}(\mathrm{Mo}) + 0.89\varphi_{2s}(\mathrm{Be}) - 0.17\varphi_{2p_z}(\mathrm{Be})$
	2σ	$0.90\varphi_{4d_{z^2}}(\mathrm{Mo}) - 0.39\varphi_{5s}(\mathrm{Mo}) - 0.16\varphi_{2p_z}(\mathrm{Be})$
	$1\delta_+$	$1.00\varphi_{4d_{x^2-y^2}}(\mathrm{Mo})$
	$1\pi_x$	$0.97\varphi_{4d_{xz}}(\mathrm{Mo}) + 0.17\varphi_{2p_x}(\mathrm{Be})$
	$2\pi_x$	$-0.21\varphi_{4d_{xz}}(\mathrm{Mo}) + 0.64\varphi_{5p_x}(\mathrm{Mo}) + 0.65\varphi_{2p_x}(\mathrm{Be})$
	$1\pi_y$	$0.97\varphi_{4d_{yz}}(\mathrm{Mo}) + 0.17\varphi_{2p_y}(\mathrm{Be})$
	$2\pi_y$	$-0.21\varphi_{4d_{yz}}(\mathrm{Mo}) + 0.64\varphi_{5p_y}(\mathrm{Mo}) + 0.65\varphi_{2p_y}(\mathrm{Be})$
	$1\delta_-$	$1.00\varphi_{4d_{xy}}(\mathrm{Mo})$
$^3\Delta(1)$	1σ	$0.32\varphi_{4d_{z^2}}(\mathrm{Mo}) + 0.64\varphi_{5s}(\mathrm{Mo}) + 0.26\varphi_{5p_z}(\mathrm{Mo}) + 0.84\varphi_{2s}(\mathrm{Be}) - 0.20\varphi_{2p_z}(\mathrm{Be})$
	2σ	$0.86\varphi_{4d_{z^2}}(\mathrm{Mo}) - 0.42\varphi_{5s}(\mathrm{Mo}) + 0.14\varphi_{5p_z}(\mathrm{Mo}) + 0.15\varphi_{2s}(\mathrm{Be}) - 0.26\varphi_{2p_z}(\mathrm{Be})$
	$1\delta_+$	$1.00\varphi_{4d_{x^2-y^2}}(\mathrm{Mo})$
	$1\pi_x$	$0.87\varphi_{4d_{xz}}(\mathrm{Mo}) + 0.43\varphi_{2p_x}(\mathrm{Be})$
	$1\pi_y$	$0.87\varphi_{4d_{yz}}(\mathrm{Mo}) + 0.43\varphi_{2p_y}(\mathrm{Be})$
	$1\delta_-$	$1.00\varphi_{4d_{xy}}(\mathrm{Mo})$
$^3\Pi(1)$	1σ	$0.46\varphi_{4d_{z^2}}(\mathrm{Mo}) + 0.68\varphi_{5s}(\mathrm{Mo}) + 0.28\varphi_{5p_z}(\mathrm{Mo}) + 0.70\varphi_{2s}(\mathrm{Be}) - 0.36\varphi_{2p_z}(\mathrm{Be})$
	2σ	$0.35\varphi_{4d_{z^2}}(\mathrm{Mo}) + 0.33\varphi_{5s}(\mathrm{Mo}) - 0.55\varphi_{2s}(\mathrm{Be}) - 0.63\varphi_{2p_z}(\mathrm{Be})$
	3σ	$0.75\varphi_{4d_{z^2}}(\mathrm{Mo}) - 0.66\varphi_{5s}(\mathrm{Mo})$
	$1\delta_+$	$1.00\varphi_{4d_{x^2-y^2}}(\mathrm{Mo})$
	$1\pi_x$	$0.93\varphi_{4d_{xz}}(\mathrm{Mo}) + 0.27\varphi_{2p_x}(\mathrm{Be})$
	$1\pi_y$	$0.93\varphi_{4d_{yz}}(\mathrm{Mo}) + 0.27\varphi_{2p_y}(\mathrm{Be})$
	$1\delta_-$	$1.00\varphi_{4d_{xy}}(\mathrm{Mo})$
$^3\Sigma^+(1)$	1σ	$0.45\varphi_{4d_{z^2}}(\mathrm{Mo}) + 0.65\varphi_{5s}(\mathrm{Mo}) + 0.26\varphi_{5p_z}(\mathrm{Mo}) + 0.71\varphi_{2s}(\mathrm{Be}) - 0.36\varphi_{2p_z}(\mathrm{Be})$
	2σ	$0.68\varphi_{4d_{z^2}}(\mathrm{Mo}) - 0.12\varphi_{5s}(\mathrm{Mo}) + 0.21\varphi_{5s}(\mathrm{Mo}) - 0.37\varphi_{2s}(\mathrm{Be}) - 0.54\varphi_{2p_z}(\mathrm{Be})$
	3σ	$-0.38\varphi_{4d_{z^2}}(\mathrm{Mo}) + 0.76\varphi_{5s}(\mathrm{Mo}) - 0.37\varphi_{2s}(\mathrm{Be}) - 0.54\varphi_{2p_z}(\mathrm{Be})$
	$1\delta_+$	$1.00\varphi_{4d_{x^2-y^2}}(\mathrm{Mo})$
	$1\pi_x$	$0.93\varphi_{4d_{xz}}(\mathrm{Mo}) + 0.27\varphi_{2p_x}(\mathrm{Be})$
	$1\pi_y$	$0.93\varphi_{4d_{yz}}(\mathrm{Mo}) + 0.27\varphi_{2p_y}(\mathrm{Be})$
	$1\delta_-$	$1.00\varphi_{4d_{xy}}(\mathrm{Mo})$
$^9\Pi(1)$	1σ	$0.22\varphi_{4d_{z^2}}(\mathrm{Mo}) + 0.43\varphi_{5s}(\mathrm{Mo}) + 0.26\varphi_{5p_z}(\mathrm{Mo}) + 0.88\varphi_{2s}(\mathrm{Be})$
	2σ	$0.73\varphi_{4d_{z^2}}(\mathrm{Mo}) - 0.68\varphi_{5s}(\mathrm{Mo}) - 0.12\varphi_{2p_z}(\mathrm{Be})$
	3σ	$0.55\varphi_{4d_{z^2}}(\mathrm{Mo}) + 0.54\varphi_{5s}(\mathrm{Mo}) - 0.37\varphi_{2s}(\mathrm{Be}) - 0.60\varphi_{2p_z}(\mathrm{Be})$
	$1\delta_+$	$1.00\varphi_{4d_{x^2-y^2}}(\mathrm{Mo})$
	$1\pi_x$	$0.97\varphi_{4d_{xz}}(\mathrm{Mo}) + 0.16\varphi_{2p_x}(\mathrm{Be})$
	$2\pi_x$	$-0.26\varphi_{4d_{xz}}(\mathrm{Mo}) + 0.36\varphi_{5p_x}(\mathrm{Mo}) + 0.74\varphi_{2p_x}(\mathrm{Be})$
	$1\pi_y$	$0.97\varphi_{4d_{yz}}(\mathrm{Mo}) + 0.16\varphi_{2p_y}(\mathrm{Be})$
	$2\pi_y$	$-0.26\varphi_{4d_{yz}}(\mathrm{Mo}) + 0.36\varphi_{5p_y}(\mathrm{Mo}) + 0.74\varphi_{2p_y}(\mathrm{Be})$
	$1\delta_-$	$1.00\varphi_{4d_{xy}}(\mathrm{Mo})$

Table 3 (*continued*)

State	Molecular orbital	Atomic orbitals
$^9\Sigma^+(1)$	1σ	$0.80\varphi_{5s}(\mathrm{Mo}) + 0.15\varphi_{4d_{z^2}}(\mathrm{Mo}) + 0.49\varphi_{2s}(\mathrm{Be}) - 0.37\varphi_{2p_z}(\mathrm{Be})$
	2σ	$-0.44\varphi_{5s}(\mathrm{Mo}) + 0.29\varphi_{5p_z}(\mathrm{Mo}) + 0.86\varphi_{2s}(\mathrm{Be}) + 0.29\varphi_{2p_z}(\mathrm{Be})$
	3σ	$-0.96\varphi_{4d_{z^2}}(\mathrm{Mo}) + 0.22\varphi_{5s}(\mathrm{Mo})$
	4σ	$0.20\varphi_{5s}(\mathrm{Mo}) - 0.93\varphi_{5p_z}(\mathrm{Mo}) + 0.82\varphi_{2p_z}(\mathrm{Be})$
	$1\delta_+$	$1.00\varphi_{4d_{x^2-y^2}}(\mathrm{Mo})$
	$1\pi_x$	$0.96\varphi_{4d_{xz}}(\mathrm{Mo}) + 0.16\varphi_{2p_x}(\mathrm{Be})$
	$1\pi_y$	$0.96\varphi_{4d_{yz}}(\mathrm{Mo}) + 0.16\varphi_{2p_y}(\mathrm{Be})$
	$1\delta_-$	$1.00\varphi_{4d_{xy}}(\mathrm{Mo})$

For these nine electronic states, their usual spectroscopic parameters, such as bond distances, dissociation energies, dipole moments, harmonic and anharmonic corrections, relative adiabatic energies at CASSCF, MRCISD and MRCISD+Q/aug-cc-pV5Z(-PP) are provided in Table 2 and their leading equilibrium CASSCF configuration accompanied by its corresponding molecular orbitals are given in Table 3. Over the following paragraphs we further discuss in detail the bonding of these selected electronic states.

3.2.1 Ground state $X^7\Sigma^+$. This state, $X^7\Sigma^+$, is clearly separated from the remaining 42 calculated states and thus it is assigned as the ground one. It correlates with the adiabatic products Mo(a^7S) + Be(^{1}S) and this character is retained in the bonding at equilibrium. It should be noted that at the CASSCF/aug-cc-pV5Z(-PP) level, the $X^7\Sigma^+$ state is nearly bound, while at the corresponding MRCISD and MRCISD+Q/aug-cc-pV5Z(-PP) level is bound in excellent agreement with the coupled cluster results, see discussion below. However, when the $X^7\Sigma^+$ state is calculated *via* a SA-CASSCF approach, *i.e.*, state average of the $X^7\Sigma^+(1)$, $^7\Sigma^+(2)$, $^7\Sigma^+(3)$, $^7\Delta(1)$, $^7\Delta(2)$, $^7\Sigma^-(1)$, and $^7\Sigma^-(2)$ states, the $X^7\Sigma^+$ state is bound with a D_e = 4.39 kcal mol^{-1}. The main equilibrium configuration of the $X^7\Sigma^+$ state at the MRCISD/aug-cc-pV5Z(-PP) level, followed by the Mulliken atomic population distributions (Mo/Be) at the MRCISD/cc-pVTZ(-PP) level, and the composition of the corresponding molecular orbitals, are: $|X^7\Sigma^+\rangle \cong 0.95|1\sigma^2 2\sigma^1 3\sigma^1 1\delta_+^1 1\pi_x^1 1\pi_y^1 1\delta_-^1\rangle$ $5s^{1.11}5p_z^{0.23}5p_x^{0.01}5p_y^{0.01}$-$4d_{z^2}^{1.00}4d_{x^2-y^2}^{0.99}4d_{xz}^{0.94}4d_{yz}^{0.94}4d_{xy}^{0.99}/2s^{1.24}2p_z^{0.31}2p_x^{0.08}2p_y^{0.08}$.

The molecular orbitals (MOs) of the valence electrons are plotted in Scheme 1a and the formed bond is summarized in the vbL diagram in Scheme 1b. MOs show that there exists an evident $4d_{z^2}5s5p_z$ hybridization of orbitals on the Mo atom, while the Be atom exhibits $2s2p_z$ hybridization, see Table 3. Based on the MOs, it is found that a σ dative-type bond formed between the $4d_{z^2}$ single electron of Mo and the vacant $2p_z$ orbital of Be, resulting in a σ half-bond with a length of 2.462 Å, and a dissociation energy of 13.85 kcal mol^{-1}, at the computational level MRCISD+Q/aug-cc-pV5Z(-PP), as shown in Table 2. Also, the $1\pi_x^1$ and $1\pi_y^1$ orbitals show that a small electron density is transferred to the empty $2p_x$ and $2p_y$ orbitals of the Be atom. Mulliken and natural population analysis at the MRCISD/aug-cc-pV5Z(-PP) levels are given in SI. NPA shows also the existence of a $2s2p_z$ hybridization on Be. All populations show that the Mo atom is in the ground state. Of course, there are some differences in the charge distributions between population analysis methods; nevertheless, it is generally accepted that both Mulliken and natural population analysis are useful for comparing similar states of the same molecule within a consistent methodological framework.[54]

The $X^7\Sigma^+$ state has been studied *via* coupled-cluster theory in ref. 42, where the ground states of the MoX molecules, where X = Li, Be, B, C, N, O, and F, have been calculated. The $X^7\Sigma^+$ state of the MoBe molecule has been calculated *via* the restricted open shell CCSD(T)[56] using the aug-cc-pV5Z(-PP) basis set[45] when the valence [$2s^2$(Be) + $5s^14d^5$(Mo)] electrons are correlated and using the aug-cc-pwCV5Z(-PP) basis set[45] when all 18 electrons treated *via ab initio*

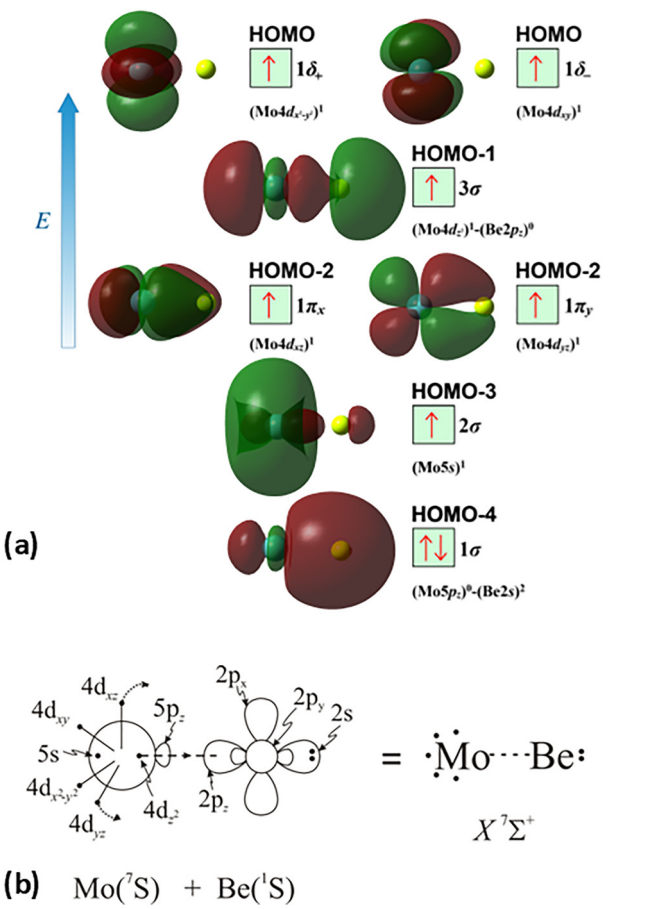

Scheme 1 (a) MOs diagrams and (b) valence bond Lewis diagram of the ground state $X^7\Sigma^+$ of MoBe at the CASSCF/aug-cc-pV5Z(-PP) level.

calculations [$1s^2 2s^2$(Be) + $4s^2 4p^6 5s^1 4d^5$(Mo)] are correlated. For reason of simplicity and in accordance with ref. 42, the methods are denoted as RCCSD(T)/aug-cc-pV5Z(-PP) and C-RCCSD(T)/aug-cc-pwCV5Z(-PP), where C- stands for core. The coupled cluster dissociation energy was calculated at 13.51 kcal mol^{-1} *via* the RCCSD(T)/aug-cc-pV5Z(-PP) method and 14.44 kcal mol^{-1} *via* C-RCCSD(T)/aug-cc-pwCV5Z(-PP).[42] The values are similar to the MRCISD+Q/aug-cc-pV5Z(-PP) value of 13.85 kcal mol^{-1}. Finally, it should be added that the correlation of the $4s^2 4p^6$ electrons of Mo and $1s^2$ electrons of Be leads to a shorter bond distance in the ground state of about 0.03 Å, see Table 2, as is expected, either at multireference level of theory or coupled cluster level of theory. To sum up, the C-RCCSD(T)/aug-cc-pwCV5Z(-PP) method provides the best D_e and r_e values, *i.e.*, D_e = 14.44 kcal mol^{-1} and r_e = 2.452 Å, for the ground state, since the $X^7\Sigma^+$ state is a single reference state. Finally, as mentioned in the computational details section, our previous calculations on the MoC molecule,[21] using either a relativistic pseudopotential on Mo (as in the present study) or an all-electron basis set to correlate core electrons including relativistic effects, showed that applying the second-order Douglas–Kroll–Hess (DKH2) approach resulted in the same bond distances and similar dissociation energies compared to those obtained with accurate core-relativistic pseudopotentials of the aug-cc-pV5Z-PP basis set.[21] Therefore, we conclude that the use of accurate core-relativistic pseudopotentials of quintuple-ζ quality effectively accounts for scalar relativistic effects.

3.2.2 First excited state $a^5\Sigma^+$. The $a^5\Sigma^+$ excited state of MoBe correlates to the Mo(a^5S) + Be(^{1}S) adiabatic atomic products, with Be lying in its ground state, whilst Mo is in its first excited one. In the equilibrium, the *in situ* atomic states differ from the adiabatic products, however the main configuration state functions (CSFs) correspond to a mix of Mo(a^5D) + Be(^{1}S), and Mo(a^7S) + Be(^{3}P). Specifically, the equilibrium CASSCF/aug-cc-pV5Z(-PP) representation of the state consists mainly of three different CSFs, listed below. These are followed by the Mulliken atomic distributions (Mo/Be), at the MRCISD/cc-pVTZ(-PP) level:

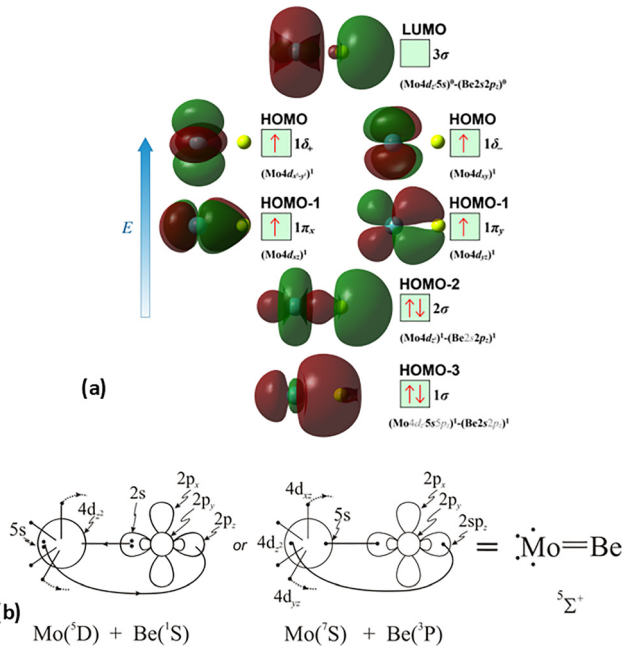

Scheme 2 (a) MOs diagrams and (b) valence bond Lewis diagram of the $a^5\Sigma^+$(1) state of MoBe at the CASSCF/aug-cc-pV5Z(-PP) level.

scenario, molybdenum, residing in its excited Mo(a^5D) state, forms with beryllium, in its ground state, Be(^{1}S), two dative σ bonds, owing to the Be atom acting as an electron density donor, transferring its 2s electron lone pair inside Mo's vacant $4d_{z^2}$ orbital, forming a dative σ bond, while the Mo atom responds by forming an additional dative σ bond, by transferring its own 5s electron lone pair inside the vacant $2p_z$ orbital of Be, resulting in a double bond. In the alternative, but equally plausible case, Mo atom is in its ground state, Mo(a^7S), whilst Be atom resides in its first excited state, Be(^{3}P). In this combination, two σ covalent bonds can form, one arising from the spin coupling between a 5s single electron of Mo with a 2s single electron of Be, and one from the spin coupling between a $4d_{z^2}$ single electron of Mo with a $2p_z$ single electron of Be,

$$|a^5\Sigma^+\rangle \cong 0.57\left|1\sigma^2 2\sigma^2 1\delta_+^1 1\pi_x^1 1\pi_y^1 1\delta_-^1\right\rangle - 0.47\left|1\sigma^2 3\sigma^2 1\delta_+^1 1\pi_x^1 1\pi_y^1 1\delta_-^1\right\rangle - +0.38\left|1\sigma^2 2\sigma^1 3\sigma^1 \overline{1\delta}_+^1 1\pi_x^1 1\pi_y^1 1\delta_-^1\right\rangle$$
$$-5s^{1.16}5p_z^{0.13}5p_x^{0.02}5p_y^{0.02}4d_{z^2}^{1.04}4d_{x^2-y^2}^{1.00}4d_{xz}^{0.94}4d_{yz}^{0.94}4d_{xy}^{0.99}/2s^{0.98}2p_z^{0.60}2p_x^{0.05}2p_y^{0.05}$$

Based on the above representation, we can assert that the $a^5\Sigma^+$ state exhibits an intent multi-reference character, at the MRCISD/aug-cc-pV5Z(-PP) level, as indicated by the relatively low reference weight (c_0 = 0.57) of the leading configuration, which reflects significant configuration mixing. Although this state correlates adiabatically to Mo(a^5S) + Be(^{1}S) at dissociation, its electronic structure near equilibrium is predominantly described by configurations corresponding to either Mo(a^5D) + Be(^{1}S) or Mo(a^7S) + Be(^{3}P). It was not possible to clarify which one is the predominant since both correspond to the same double σ bond ($1\sigma^2 2\sigma^2$). However, the origin of the electrons forms the double bond differ, see Scheme 2b. In the first giving rise to a double bond, as well. A superposition between these two configurations exists at equilibrium. Population analysis shows that about 0.4e^- is transferred from Be to Mo in the σ frame, *i.e.*, the Mo/Be is: $5s^{1.16}5p_z^{0.13}$-$4d_{z^2}^{1.04}/2s^{0.98}2p_z^{0.60}$ while, it is evident that a $4d_{z^2}5s5p_z$ hybridization exists on the Mo atom, and a $2s2p_z$ hybridization on Be atom. However, it can be regarded as a more likely scenario the Mo(a^7S) + Be(^{3}P) combination, since two covalent bonds may be more favorable than two dative or because in the case of two dative bonds it is not likely to be transferred one electron to the empty $4d_{z^2}^0$ of Mo. Finally, a small electron density is transferred to the empty $2p_x$ and $2p_y$ orbitals of the Be atom from the $1\pi_x^1$

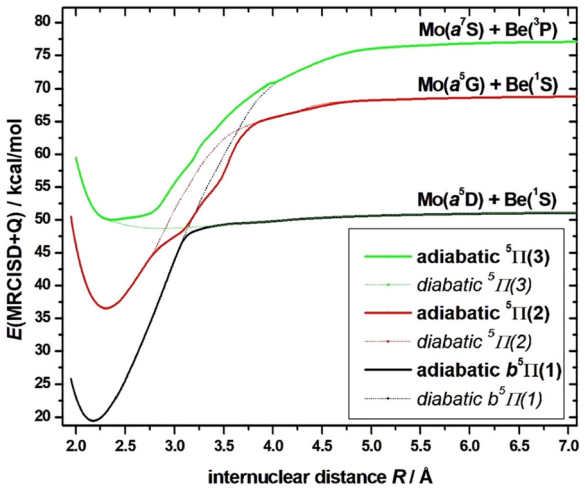

Fig. 6 PECs of the adiabatic and diabatic $b^5\Pi$, $^5\Pi(2)$, and $^5\Pi(3)$ states of MoBe at the MRCISD+Q/aug-cc-pV5Z(-PP) computational level. The equilibrium minimum of the ground state $X^7\Sigma^+$ is used to define the zero of energy.

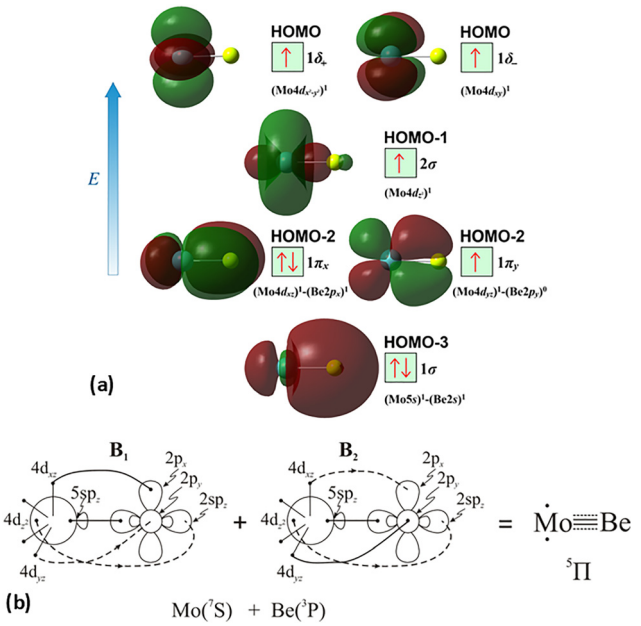

Scheme 3 (a) MOs diagrams and (b) valence bond Lewis diagram of the $b^5\Pi(1)$ state of MoBe at the CASSCF/aug-cc-pV5Z(-PP) level.

and $1\pi_y^1$ orbitals and as a result a total of about 0.26*e* are transferred from Be to Mo.

At the MRCISD+Q/aug-cc-pV5Z(-PP) level of theory, the $a^5\Sigma^+$ state has a bond length of 2.393 Å, and an adiabatic dissociation energy of 28.20 kcal mol^{-1}. The diabatic dissociation energy can be estimated by adjusting the adiabatic dissociation energy: specifically, by subtracting the energy required for Mo(a^{5}S) to relax back to its ground state, Mo(a^7S), and adding the excitation energy needed for Be(^{1}S) to transition to its triplet first excited state, Be(^{3}P). This yields a diabatic D_e of 60.25 kcal mol^{-1} = {28.20–30.79[Mo(a^7S) ← Mo(a^5S)] + 62.84[Be(^{1}S) → Be(^{3}P)]} kcal mol^{-1}.[57,58] Interestingly, when referenced to the Mo(a^5D) + Be(^{1}S) atomic limit, the diabatic dissociation energy is of the same order, of 62.03 kcal mol^{-1} {= 28.00 kcal mol^{-1}, +33.83 Mo(a^5S) → Mo(a^5D)}, reinforcing the equivalence between the two alternative configurations. Based on the dissociation energies, a relatively strong covalent bond must form between the two atoms, as expected from the bond order.

3.2.3 Second excited state b$^5\Pi$. The $b^5\Pi$ excited state of MoBe correlates with the Mo(a^5D) + Be(^{1}S) adiabatic atomic limit, however, it does not retain this character along the entire PEC. At about 3 Å, an avoided crossing takes place, with an excited $^5\Pi(2)$ state, that correlates with the Mo(a^5G) + Be(^{1}S) adiabatic atomic limit, which, in turn, couples with the excited $^5\Pi(3)$ state, that correlates with the Mo(a^7S) + Be(^{3}P) adiabatic atomic limit, which showcases an additional avoided crossing, at about 4 Å, intertwining this lot of three states, see Fig. 2, 5 and 6. Thus, in equilibrium, the configurations of the atoms forming the bond of the $b^5\Pi$ excited state reside in the Mo(a^7S) + Li(^{3}P) atomic states. In Fig. 6, both the adiabatic and diabatic PECs of $b^5\Pi$, $^5\Pi(2)$, and $^5\Pi(3)$ states have been plotted, where the avoided crossings are clearly observed.

At the equilibrium minimum of the b$^5\Pi$ state, the leading equilibrium CASSCF configuration, followed by the Mulliken atomic distributions (Mo/Be) are:

$$|b^5\Pi\rangle \cong \frac{0.83}{\sqrt{2}}\left\{\left|1\sigma^2 2\sigma^1 1\delta_+^1 1\pi_x^2 1\pi_y^1 1\delta_-^1\right\rangle + \left|1\sigma^2 2\sigma^1 1\delta_+^1 1\pi_x^1 1\pi_y^2 1\delta_-^1\right\rangle\right\}$$

$$5s^{0.94}5p_z^{0.19}5p_x^{0.04}5p_y^{0.01}4d_{z^2}^{0.95}4d_{x^2-y^2}^{1.02}4d_{xz}^{1.33}4d_{yz}^{0.91}$$
$$4d_{xy}^{0.99}/2s^{0.81}2p_z^{0.60}2p_x^{0.60}2p_y^{0.10} \quad B_1$$

$$5s^{0.94}5p_z^{0.19}5p_x^{0.01}5p_y^{0.04}4d_{z^2}^{0.95}4d_{x^2-y^2}^{1.02}4d_{xz}^{0.91}4d_{yz}^{1.33}$$
$$4d_{xy}^{0.99}/2s^{0.81}2p_z^{0.60}2p_x^{0.10}2p_y^{0.60} \quad B_2$$

The plot of valence MOs and vbL diagram of the bonding are depicted in Scheme 3. The bonding is based on the leading CSF, the atomic Mulliken distributions, and the molecular orbitals' composition seen on Table 3. Namely, the Mo(^{7}S) atom forms a σ covalent bond with the Be(^{3}P) atom, $5s^1$(Mo)–$2s^1$(Be), a σ half-bond, from the dislocation of Mo's $4d_{z^2}$ single electron inside the vacant $2p_z$ atomic orbital of Be, $4d_{z^2}{}^1$(Mo)–$2p_z^0$(Be), and, additionally it is formed a π^2 covalent bond and a π^1 dative bond, either $4d_{xz}^1$(Mo)–$2p_x^1$(Be) and $4d_{yz}^1$(Mo)–$2p_y^0$ orbital of Be, or $4d_{xz}^1$(Mo)–$2p_x^0$(Be) and $4d_{yz}^1$(Mo)–$2p_y^1$(Be). Again, a strong $4d_{z^2}5s5p_z$ hybridization is prevalent on the Mo atom. Overall, a total of about 0.38*e* are transferred from the Be atom to the Mo metal.

Thus, a bond of order 3, $\sigma^2\sigma^1\pi^2\pi^1$, with a bond length of 2.177 Å is formed with an adiabatic dissociation energy of 57.72 kcal mol^{-1}, at the MRCISD+Q/aug-cc-pV5Z(-PP) level of theory. The diabatic dissociation energy, *i.e.*, the energy with respect to the *in situ* atoms, can be estimated by adjusting the adiabatic dissociation energy, by subtracting the energy required

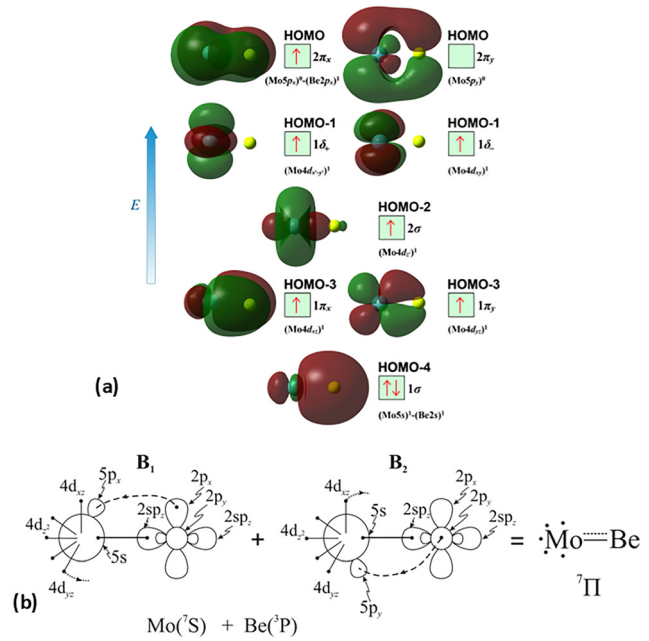

Scheme 4 (a) MOs diagrams and (b) valence bond Lewis diagram of the $A^7\Pi(1)$ state of MoBe at the CASSCF/aug-cc-pV5Z(-PP) level.

for Mo(a^5D) to relax back to its ground state, Mo(a^7S), and adding the excitation energy needed for Be(^{1}S) to transition to its triplet first excited state, Be(^{3}P); D_e = 86.73 kcal mol^{-1} = {57.72–33.83[Mo(a^7S) ← Mo(a^5D)] + 62.84[Be(^{1}S) → Be(^{3}P)]}.[57,58] Based on this dissociation energy, we conclude that a strong covalent bond is formed between the two atoms, as expected from the high bond order.

3.2.4 Third excited state $A^7\Pi$. The $A^7\Pi$ excited state of MoBe correlates to the Mo(a^7S) + Be(^{3}P) adiabatic atomic products and retains this character in equilibrium. The leading equilibrium CASSCF configuration, followed by the Mulliken atomic distributions (Mo/Be) are:

$$|A^7\Pi\rangle \cong \frac{0.94}{\sqrt{2}} \times \left\{\left|1\sigma^2 2\sigma^1 1\delta_+^1 1\pi_x^1 2\pi_x^1 1\pi_y^1 1\delta_-^1\right\rangle + \left|1\sigma^2 2\sigma^1 1\delta_+^1 1\pi_x^1 1\pi_y^1 2\pi_y^1 1\delta_-^1\right\rangle\right\}$$

$$5s^{0.78}5p_z^{0.20}5p_x^{0.38}5p_y^{0.01}4d_{z^2}^{0.96}4d_{x^2-y^2}^{1.00}4d_{xz}^{0.97}4d_{yz}^{0.95} 4d_{xy}^{0.99}/2s^{0.94}2p_z^{0.07}2p_x^{0.64}2p_y^{0.06} \quad B_1$$

$$5s^{0.78}5p_z^{0.20}5p_x^{0.01}5p_y^{0.38}4d_{z^2}^{0.96}4d_{x^2-y^2}^{1.00}4d_{xz}^{0.95}4d_{yz}^{0.97} 4d_{xy}^{0.99}/2s^{0.94}2p_z^{0.07}2p_x^{0.06}2p_y^{0.64} \quad B_2$$

The bonding in this state is summarized in the vbL diagram of Scheme 4. Namely, a σ^2 covalent bond is formed, 5s^1(Mo)–2s^1(Be), and a π^1 half-bond either a $5p_x^0$(Mo)–$2p_x^1$(Be) or $5p_y^0$(Mo)–$2p_y^1$(Be). Likewise, a $4d_{z^2}5s5p_z$ hybridization is observed at the Mo atom. Overall, a total electron charge of about 0.25e is transferred from the Be atom to the Mo metal. The resulting $\sigma^2\pi^1$ bond has an order of 1.5, a bond length of 2.359 Å, and a

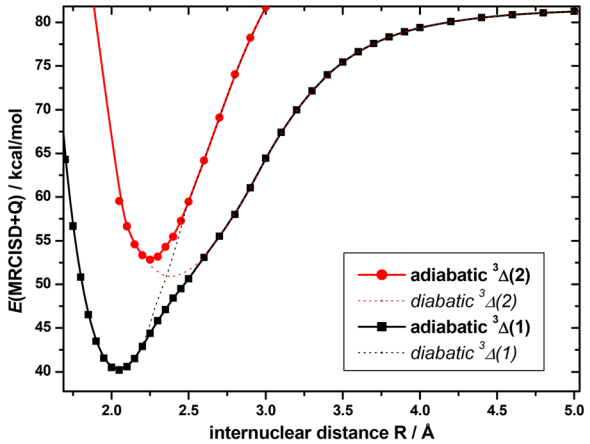

Fig. 7 PECs of the adiabatic and diabatic $^3\Delta(1)$, and $^3\Delta(2)$ states of MoBe at the MRCISD+Q/aug-cc-pV5Z(-PP) computational level. The equilibrium minimum of the ground state $X^7\Sigma^+$ is used to define the zero of energy.

dissociation energy of 42.3 kcal mol^{-1}, at the MRCISD+Q/aug-cc-pV5Z(-PP) level of theory.

3.2.5 $^3\Delta(1)$. The $^3\Delta(1)$ excited state of MoBe correlates with the Mo(a^3G; 4d^5(^{4}G)5s^1) + Be(^{1}S; 2s^2) adiabatic atomic limit, however, it does not retain this character along the entire PEC. At about 2.4 Å, an avoided crossing is observed with an excited, $^3\Delta(2)$ state, that correlates with the Mo(a^5G; 4d^5(^{4}G)5s^1) + Be(^{3}P; 2s^{1}2p^1) atomic limit, see Fig. 7 where both the adiabatic and diabatic PECs of $^3\Delta(1)$, and $^3\Delta(2)$ states have been plotted.

At the equilibrium minimum of the $^3\Delta(1)$ state, the leading equilibrium CASSCF configuration, followed by the Mulliken atomic distributions (Mo/Be) are:

$$|^3\Delta(1)\rangle \cong 0.88\left\{\frac{1}{\sqrt{2}}\left|1\sigma^2 2\sigma^1 1\delta_+^1 1\pi_x^2 1\pi_y^2\right\rangle + \frac{1}{\sqrt{2}}\left|1\sigma^2 2\sigma^1 1\pi_x^2 1\pi_y^2 1\delta_-^1\right\rangle\right\}$$

$$5s^{1.14}5p_z^{0.18}5p_x^{0.03}5p_y^{0.03}4d_{z^2}^{0.95}4d_{x^2-y^2}^{1.00}4d_{xz}^{1.53}4d_{yz}^{1.53} 4d_{xy}^{0.07}/2s^{0.65}2p_z^{0.06}2p_x^{0.37}2p_y^{0.37} \quad A_1$$

$$5s^{1.14}5p_z^{0.18}5p_x^{0.03}5p_y^{0.03}4d_{z^2}^{0.95}4d_{x^2-y^2}^{0.07}4d_{xz}^{1.53}4d_{yz}^{1.53} 4d_{xy}^{1.00}/2s^{0.65}2p_z^{0.06}2p_x^{0.37}2p_y^{0.37} \quad A_2$$

The bonding is formed between the ^{3}P state of Be and the a^5G excited state of Mo, resulting in three bonds, $\sigma^2\pi^2\pi^2$. Specifically, a covalent σ^2 bond is formed, 5s^1(Mo)–2s^1(Be), one π^2 covalent bond and one π^2 dative bond, either $4d_{xz}^1$(Mo)–$2p_x^1$(Be) and $4d_{yz}^2$(Mo) → $2p_y^0$(Be) or $4d_{yz}^1$(Mo)–$2p_y^1$(Be) or $4d_{xz}^2$(Mo) → $2p_x^0$(Be), see Scheme 5. Hybridizations on both Mo and B are present, *i.e.*, $4d_{z^2}5s5p_z$ and $2s2p_z$, while about 0.49e are transferred from the Be atom to the Mo metal (Scheme 5).

This state presents the shortest bond distance and the largest diabatic dissociation energy among the calculated states. The bond distance is 2.047 Å, the adiabatic D_e value is 41.84 kcal mol^{-1}, at the MRCISD+Q/aug-cc-pV5Z(-PP) level of theory, whilst its diabatic dissociation energy is 92.01 kcal mol^{-1} {= 41.84–12.67[Mo(a^5G) ← Mo(a^3G)] + 62.84[Be(^{1}S) → Be(^{3}P)]} kcal mol^{-1}.[57,58]

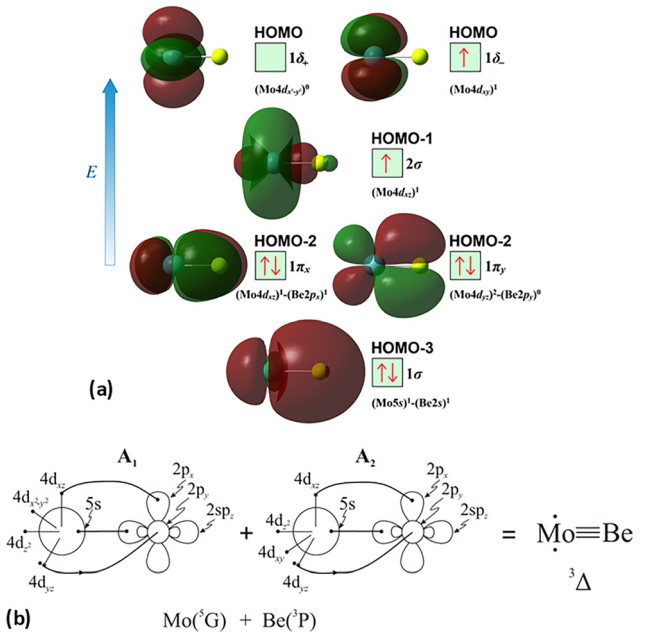

Scheme 5 (a) MOs diagrams and (b) valence bond Lewis diagram of the $^3\Delta(1)$ state of MoBe at the CASSCF/aug-cc-pV5Z(-PP) level.

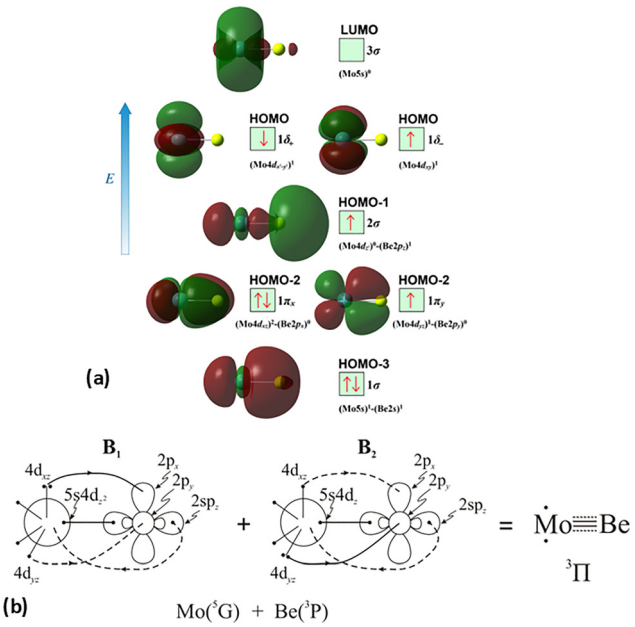

Scheme 6 (a) MOs diagrams and (b) valence bond Lewis diagram of the $^3\Pi(1)$ state of MoBe at the CASSCF/aug-cc-pV5Z(-PP) level.

3.2.6 $^3\Pi(1)$. The $^3\Pi(1)$ excited state of MoBe, similarly to the $^3\Delta(1)$ one before, correlates to the Mo(a^3G) + Be(^{1}S) while in the equilibrium the bonding the *in situ* atoms are: Mo(a^5G) + Be(^{3}P). The equilibrium CASSCF representation of the state consists mainly of two different CSFs, listed below. These are followed by the Mulliken atomic distributions (Mo/Be), at the MRCISD/cc-pVTZ level:

$$|^3\Pi(1)\rangle \cong 0.55\left\{\frac{1}{\sqrt{2}}\left|1\sigma^2 2\sigma^1 \overline{1\delta}^1_+ 1\pi^2_x 1\pi^1_y 1\delta^1_-\right\rangle + \frac{1}{\sqrt{2}}\left|1\sigma^2 2\sigma^1 \overline{1\delta}^1_+ 1\pi^1_x 1\pi^2_y 1\delta^1_-\right\rangle\right\}$$
$$+ 0.35\left\{\frac{1}{\sqrt{2}}\left|1\sigma^2 2\sigma^1 3\sigma^1 \overline{1\delta}^1_+ 1\pi^1_x 1\pi^2_y\right\rangle + \frac{1}{\sqrt{2}}\left|1\sigma^2 2\sigma^1 3\sigma^1 \overline{1\delta}^1_+ 1\pi^2_x 1\pi^1_y\right\rangle\right\}$$

$$5s^{1.10}5p_z^{0.16}5p_x^{0.03}5p_y^{0.02}4d_{z^2}^{0.78}4d_{x^2-y^2}^{0.79}4d_{xz}^{1.48}4d_{yz}^{1.08}$$
$$4d_{xy}^{0.80}/2s^{0.89}2p_z^{0.49}2p_x^{0.21}2p_y^{0.10} \quad B_1$$

$$5s^{1.10}5p_z^{0.16}5p_x^{0.02}5p_y^{0.03}4d_{z^2}^{0.78}4d_{x^2-y^2}^{0.79}4d_{xz}^{1.08}4d_{yz}^{1.48}$$
$$4d_{xy}^{0.80}/2s^{0.89}2p_z^{0.49}2p_x^{0.10}2p_y^{0.21} \quad B_2$$

The $^3\Pi$ state has a strong multi-reference character as indicated by the relatively small coefficient (c_0 = 0.55) of the leading configuration. This change in asymptotic character occurs due to the internally mixed nature of the state. The bonding in this state is summarized in Scheme 6. The bonding consists of a σ^2 covalent bond $5s^1$(Mo)–$2s^1$(Be), a σ^1 dative bond $5s4d^0_{z^2}$(hybrid orbital; Mo) ← $2s2p^1_z$(hybrid orbital; Be), and two dative $\pi^2\pi^1$ bonds, either d^2_{xz}(Mo) → $2p^0_x$(Be) and $4d^0_{yz}$(Mo) ← $2p^1_y$(Be) or d^2_{yz}(Mo) → $2p^0_y$(Be) and $4d^0_{xz}$(Mo) ← $2p^1_x$(Be). About 0.26*e* are transferred from the Be atom to the Mo metal. The resulting $\sigma^2\sigma^1\pi^2\pi^1$ bond has an order of 3, a bond length of 2.266 Å, and a dissociation energy of 37.81 kcal mol^{-1}, at the MRCISD+Q/aug-cc-pV5Z(-PP) level of theory, whilst its diabatic dissociation is 87.98 kcal mol^{-1} {= 37.81–12.67[Mo(a^5G) ← Mo(a^3G)] + 62.84[Be(^{1}S) → Be(^{3}P)]}.[57,58]

3.2.7 $^3\Sigma^+(1)$. Similarly to the two previous cases of the lowest-lying triplet bunch, the $^3\Sigma^+(1)$ excited state of MoBe correlates to the Mo(a^3G) + Be(^{1}S) adiabatic atomic limit, while in equilibrium, the bonding is formed between Mo(a^5S) + Be(^{3}P) states. Specifically, the equilibrium CASSCF representation of the state consists of various CSFs and the atomic distributions (Mo/Be) are:

$$|^3\Sigma^+(1)\rangle \cong 0.47\left|1\sigma^2 2\sigma^1 3\sigma^1 1\delta^1_+ \overline{1\pi}^1_x \overline{1\pi}^1_y 1\delta^1_-\right\rangle$$
$$- 0.46\left|1\sigma^2 \overline{2\sigma}^1 3\sigma^1 1\delta^1_+ \overline{1\pi}^1_x 1\pi^1_y 1\delta^1_-\right\rangle$$
$$- 0.28\left|1\sigma^2 2\sigma^2 1\delta^1_+ \overline{1\pi}^1_x 1\pi^1_y 1\delta^1_-\right\rangle$$
$$+ 0.22\left|1\sigma^2 2\sigma^2 1\delta^1_+ 1\pi^1_x 1\pi^1_y \overline{1\delta}^1_-\right\rangle$$

$$5s^{1.23}5p_z^{0.16}5p_x^{0.02}5p_y^{0.02}4d_{z^2}^{1.04}4d_{x^2-y^2}^{0.99}4d_{xz}^{0.88}4d_{yz}^{0.88}$$
$$4d_{xy}^{0.99}/2s^{0.97}2p_z^{0.52}2p_x^{0.10}2p_y^{0.10} \quad A_1$$

The $^3\Sigma^+(1)$ has a strongly multi-reference character indicating the presence of configuration mixing. Although this state correlates adiabatically to Mo(a^3G) + Be(^{1}S) at dissociation, its electronic structure near equilibrium is predominantly described by configurations corresponding to Mo(a^5S) + Be(^{3}P). Two covalent $\sigma^2\sigma^2$ bonds are formed, *i.e.*,

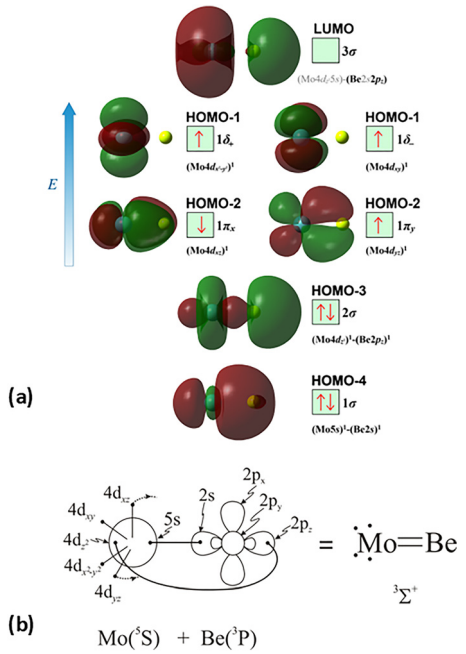

Scheme 7 (a) MOs diagrams and (b) valence bond Lewis diagram of the $^3\Sigma^+(1)$ state of MoBe at the CASSCF/aug-cc-pV5Z(-PP) level.

$5s^1$(Mo)–$2s^1$(Be) and $4d^1_{z^2}$(Mo) ← $2p^1_z$(Be) and ∼0.26*e* are transferred from Be to Mo, see Scheme 7. The bond distance is 2.333 Å and the adiabatic D_e values is 34.12 kcal mol^{-1} at MRCISD+Q/aug-cc-pV5Z(-PP). The diabatic dissociation energy is D_e (diabatic) = 67.20 kcal mol^{-1} {= 34.12–29.76[Mo(a^5S) ← Mo(a^3G) + 62.84[Be(^{1}S) → Be(^{3}P)]}.

3.2.8 $^9\Pi(1)$ and $^9\Sigma^+(1)$. The $^9\Pi(1)$ and $^9\Sigma^+(1)$ states of MoBe correlate to the Mo(a^7S) + Be(^{3}P) adiabatic atomic products, as well, and these atomic states are retained in the bonding. The leading equilibrium CASSCF configuration and the atomic distributions (Mo/Be) are:

$$|^9\Pi(1)\rangle \cong 0.98\left\{\frac{1}{\sqrt{2}}\left|1\sigma^1 2\sigma^1 3\sigma^1 1\delta_+^1 1\pi_x^1 2\pi_x^1 1\pi_y^1 1\delta_-^1\right\rangle + \frac{1}{\sqrt{2}}\left|1\sigma^1 2\sigma^1 3\sigma^1 1\delta_+^1 1\pi_x^1 1\pi_y^1 2\pi_y^1 1\delta_-^1\right\rangle\right\}$$

$$5s^{0.78}5p_z^{0.10}5p_x^{0.25}5p_y^{0.01}4d_{z^2}^{0.89}4d_{x^2-y^2}^{0.98}4d_{xz}^{0.98}4d_{yz}^{0.94}4d_{xy}^{0.99}/2s^{0.82}2p_z^{0.49}2p_x^{0.75}2p_y^{0.04}\quad B_1$$

$$5s^{0.78}5p_z^{0.10}5p_x^{0.01}5p_y^{0.25}4d_{z^2}^{0.89}4d_{x^2-y^2}^{0.99}4d_{xz}^{0.94}4d_{yz}^{0.98}4d_{xy}^{0.99}/2s^{0.82}2p_z^{0.49}2p_x^{0.04}2p_y^{0.75}\quad B_2$$

and $|^9\Sigma^+(1)\rangle \cong 0.97|1\sigma^1 2\sigma^1 3\sigma^1 4\sigma^1 1\delta_+^1 1\pi_x^1 1\pi_y^1 1\delta_-^1\rangle$

$$5s^{0.97}5p_z^{0.42}5p_x^{0.02}5p_y^{0.02}4d_{z^2}^{0.94}4d_{x^2-y^2}^{0.99}4d_{xz}^{0.92}4d_{yz}^{0.92}4d_{xy}^{0.99}/2s^{0.87}2p_z^{0.75}2p_x^{0.05}2p_y^{0.05}\quad A_1$$

In the $^9\Pi(1)$ state, two weak dative interactions are formed, *i.e.*, σ^1: $5s^1$(Mo) → $2p_z^0$(Be) and π^1: $5p_x^0$(Mo)···$2p_x^1$(Be) or $5p_y^0$(Mo)···$2p_y^1$(Be), see Scheme 8. Note that a $4d_{z^2}5s5p_z$ hybridization exists on the Mo atom and a $2s2p_z$ on Be. The calculated r_e is 2.579 Å and the D_e is 10.43 kcal mol^{-1} at the MRCISD+Q/aug-cc-pV5Z(-PP) method. The $^9\Sigma^+(1)$ state is clearly a van der Waals state, there is a $5p_z^0$(Mo)···$2s2p_z^1$(Be) interaction resulting in a

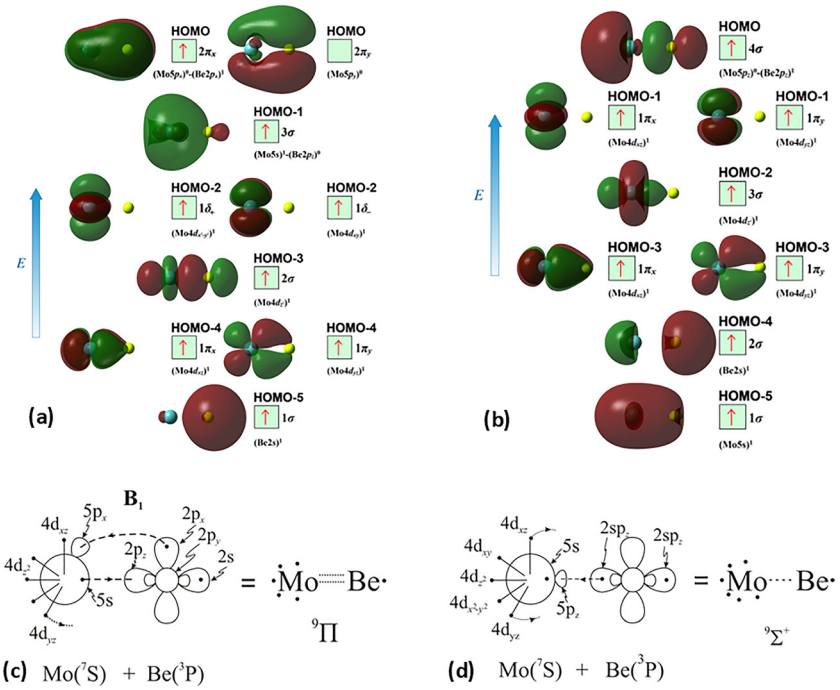

Scheme 8 (a) MOs diagrams of the $^9\Pi(1)$ state, (b) MOs diagrams of the $^9\Sigma^+(1)$ state, (c) valence bond Lewis diagram of the $^9\Pi(1)$ state, and (d) valence bond Lewis diagram of the $^9\Sigma^+(1)$ state of MoBe at the CASSCF/aug-cc-pV5Z(-PP) level.

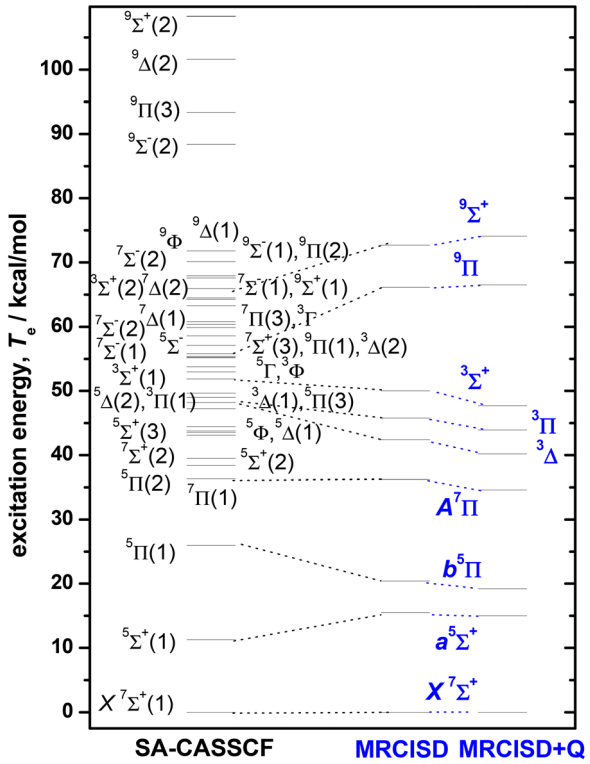

Fig. 8 Relative energy levels of all computed electronic states of MoBe.

bond distance of 2.787 Å and a dissociation energy of 2.48 kcal mol^{-1} at the MRCISD+Q/aug-cc-pV5Z(-PP) level of theory.

3.2.9 Trends and electronic spectra. The adiabatic excitation energies, *i.e.*, relative energy levels of the 43 calculated electronic states at the SA-CASSCF, MRCISD and MRCISD+Q levels are depicted in Fig. 8. It is found that while the four lowest energy states are clearly separated for the remaining excited states in all three methods, the electronic spectrum in the area that ranges from 40 kcal mol^{-1} (≈1.7 eV) to 70 kcal mol^{-1} (≈3 eV) is very dense. Some states present avoided crossing at different geometries. Namely, at the SA-CASSCF/aug-cc-pV5Z(-PP) level, many avoided crossings occur in the area 2.3–2.9 Å due to the fact that the electronic spectrum is very dense. So, $^3\Pi(2)$ present avoided crossing with $^3\Pi(3)$, $^3\Delta(1)$ with $^3\Delta(2)$, $^3\Delta(2)$ with $^3\Delta(3)$, $^3\Phi(1)$ with a higher $^3\Phi(2)$ state, $^3\Sigma^-(1)$ with a higher $^3\Sigma^-(2)$ state, $^5\Pi(1)$ with $^5\Pi(2)$, and $^5\Phi(1)$, also, with a higher $^5\Phi(2)$ one, $^5\Sigma^+(2)$ with $^5\Sigma^+(3)$, $^5\Gamma(1)$ with a higher $^5\Gamma(2)$ one, $^5\Pi(2)$ with $^5\Pi(3)$, $^5\Delta(1)$ with $^5\Delta(2)$, and $^3\Delta(2)$ with a higher $^3\Delta(2)$ state, *etc.*

Table 4 lists the nine MRCISD(+Q) calculated states along with their equilibrium products and asymptotic limits. Only four out of nine, *i.e.* $X^5\Sigma^+$, $A^7\Pi$, $^9\Pi(1)$, and $^9\Sigma^+(1)$ are single-reference states, while their equilibrium products coincide with their dissociation atomic limits. The remaining five states, $a^5\Sigma^+$, $b^5\Pi$, $^3\Pi(1)$, $^3\Sigma^+(1)$, and $^3\Delta(1)$, exhibit avoided crossing; thus equilibrium products differ from their adiabatic dissociation atomic limits, see Table 4 and they present a multireference character. Specifically, the $a^5\Sigma^+$, $^3\Pi(1)$, and $^3\Sigma^+(1)$ states

Table 4 Dissociation energies, bonding, equilibrium products, and asymptotic products of nine selected calculated states of the MoBe molecule at the MRCISD(+Q)/aug-cc-pV5Z(-PP) method

State	D_e ($D_e^{diabatic}$)	Bonding	Equilibrium products	Asymptotic products
$X^7\Sigma^+$	13.9	σ^1	Mo(a^7S) + Be(^1S)	Mo(a^7S) + Be(^1S)
$a^5\Sigma^+$	28.2 (60.3)	$\sigma^2\sigma^2$	Mo(a^7S) + Be(^3P)	Mo(a^5S) + Be(^1S)
$b^5\Pi$	57.7 (86.7)	$\sigma^2\sigma^1\pi^2\pi^1$	Mo(a^7S) + Be(^3P)	Mo(a^5D) + Be(^1S)
$A^7\Pi$	42.3	$\sigma^2\pi^1$	Mo(a^7S) + Be(^3P)	Mo(a^7S) + Be(^3P)
$^3\Delta(1)$	41.8 (92.0)	$\sigma^2\pi^2\pi^2$	Mo(a^5G) + Be(^3P)	Mo(a^3G) + Be(^1S)
$^3\Pi(1)$	37.8 (88.0)	$\sigma^2\sigma^1\pi^2\pi^1$	Mo(a^5G) + Be(^3P)	Mo(a^3G) + Be(^1S)
$^3\Sigma^+(1)$	34.1 (67.2)	$\sigma^2\sigma^2$	Mo(a^5S) + Be(^3P)	Mo(a^3G) + Be(^1S)
$^9\Pi(1)$	10.4	vdW: $(\sigma\ \pi)^a$	Mo(a^7S) + Be(^3P)	Mo(a^7S) + Be(^3P)
$^9\Sigma^+(1)$	2.5	vdW: $(\sigma)^a$	Mo(a^7S) + Be(^3P)	Mo(a^7S) + Be(^3P)

[a] van der Waals interaction, the symmetry of the interaction is given parenthesis.

present a strong multi-reference character, *i.e.*, the coefficient of their main CSF is 0.57, 0.55 and 0.47, respectively.

Regarding the calculation of the dissociation energy, the adiabatic D_e of calculated states range from 2.5 kcal mol^{-1} to 57.7 kcal mol^{-1}. The bonding ranges from van der Waals interactions to triple bonds. Note that the three states, namely $b^5\Pi$, $^3\Delta(1)$, and $^3\Pi(1)$, which have triple bonds, present avoided crossings and thus their diabatic D_e values, which are directly related with the strength of the bonding, are 86.7, 92.0 and 88.0 kcal mol^{-1}, respectively. Interestingly, the bonding schemes behind the triplet and quintet states appear to be indistinguishable (apart from spins); *i.e.* the bonding scheme of $a^5\Sigma^+$ is identical to that of $^3\Sigma^+(1)$, and the bonding scheme of $b^5\Pi$ is identical to that of $^3\Pi(1)$. Generally, in most states, electron charge is transferred from Be to Mo *via* the bonding, since the Be atom is the electropositive participating element. Finally, the corresponding bond distances range from 2.047 Å [$^3\Delta(1)$] to 2.787 Å [$^9\Sigma^+(1)$] in accordance with the size of the bond order.

Overall, the correlation between bond distances, bond order and dissociation energies are depicted in Fig. 9 and specifically, how the bonding affects them. While the Be atom possesses a closed shell valence configuration, it can participate in a multitude of bond schemes, *i.e.*, offering and receiving half bonds, offering and receiving dative bonds, and forming covalent bonds. More specifically, in its ground state (^1S), it can receive electron density in its vacant 2p valence orbitals, or offer its 2s electron lone pair density, and in its first excited state (^3P), it can use its 2s, and possibly 2p, electron's spin for coupling, or have its 2p valence orbitals available for reception of electron density. In the MoBe molecule, it was found that it forms from weak interactions such as van der Waals (in $^9\Sigma^+(1)$) and half-bond (in $X^7\Sigma^+$) or as high as triple bonds (in $b^5\Pi(1)$, $^3\Delta(1)$, and $^3\Pi(1)$ states), see Fig. 9. It's noteworthy that, in most cases, it is found that the Be atom forms bonds in its first excited state; Be(^3P). In most states, a $2s2p_z$ hybridization is assumed on Be, while a $4d_{z^2}5s5p_z$ hybridization is assumed on Mo, and, in some cases, where the Be atom assumes no hybridization, Mo still showcases the same $4d_{z^2}5s5p_z$ hybridization, by itself (*i.e.* $b^5\Pi$ and $A^7\Pi$). The bond distances of the calculated states range

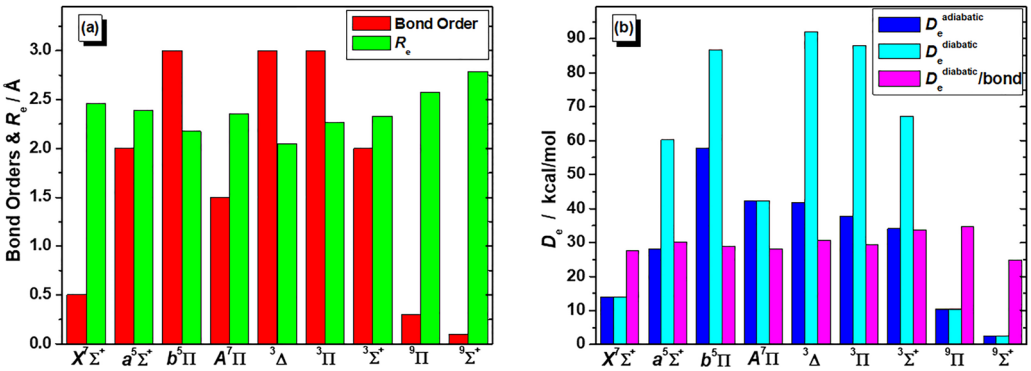

Fig. 9 (a) Bond order magnitudes and bond distances, (b) adiabatic dissociation energies, diabatic dissociation energies and diabatic dissociation energies/bond of 9 calculated states of MoBe at the MRCISD+Q/aug-cc-pV5Z(-PP) level.

from as low as 2.047 Å, in $^3\Delta(1)$, as far as 2.787 Å, in $^9\Sigma^+(1)$, see Table 2, and Fig. 9. Generally, it is observed that the excited Be(^{3}P) atom forms the shortest bonds, partially because its 2s orbital can accept easily electron density from the $4d_{z^2}5s5p_z$ orbitals of Mo, and thus form strong σ bonds, and partially owing to its capability of forming bonds both along the molecular axis, as well as laterally to it, resulting in strong bonds of high orders.

The adiabatic dissociation energies are depicted in Fig. 9. Additionally, the dissociation energy per bond, which corresponds to the bond strength, is obtained if the diabatic (related to the contributing towards bonding atomic configurations) dissociation energy is divided by the bond order 0.5 (half bond σ^1 or π^1 to 3). Regarding nonet $^9\Pi(1)$ and $^9\Sigma^+(1)$ states, the $^9\Sigma^+(1)$ is clearly a van der Waals state, while in the $^9\Pi(1)$ there is a weak interaction *via* σ and π frame. We can assume that each interaction is ∼10% the strength of typical Mo–Be covalent or dative bonds. Generally, it is considered that, the upper bound of a vdW interaction [alkyl···alkyl] is 5% of a typical covalent bond (*e.g.* C–H bond) and 7–20% of a typical dative bond (*e.g.* N→B bond), while the upper bound of a hydrogen bond (H···O) is 20% of the covalent bond;[59] however, these % values correspond in bonds from different two atoms and for the same atoms like in our case. Thus, in the Mo–Be diatomic molecule, where the vdW interaction stronger than a typical alkyl···alkyl interaction, the estimation of each interaction as the ∼10% the strength of typical Mo–Be two electron bond is reasonable. It is interesting that in all calculated states, on average, the dissociation energy per bond of the seven calculated states is 29.8 kcal mol^{-1}. Moreover, the corresponding value of the nine states, *i.e.* including also the two nonet states, is again 29.8 kcal mol^{-1}, see Fig. 9. To sum up, we have concluded that the final value for a two-electron Mo–Be bond is 30 kcal mol^{-1}.

3.2.10 Mo–Be bonds beyond diatomic molecule. Up to now, Mo–Be clusters have not been reported, however, the distinct chemistries of molybdenum and beryllium suggest potential avenues for research. The electron-deficient nature of beryllium and its ability to form multicenter bonds, combined with molybdenum's versatility in cluster formation could lead to novel Mo–Be cluster architectures. The present study will provide details regarding binding energies, *i.e.*, the formation of a two electrons Mo–Be bond corresponds to about 30 kcal mol^{-1}, bond distances that depending on the type can range from 2.05 Å to 2.90 Å, as well as it will be useful in the evaluation of similar properties within MoBe complexes.

Compounds containing interacting molybdenum and beryllium components in the bulk phase have been the focus of ongoing research for some time now, whether they be alloys, co-joint materials or interfaces and absorbed layers, aiming to identify their physical properties.[7–14] Despite this, thorough inspection of the bonding taking place in these cases has been overlooked up until now, and there are no points of reference in order to identify bonding schemes or even predict them in such materials. Thus, shedding some light into the details of the interactions between molybdenum and beryllium in solid-state systems and diffuse of either Mo or Be in a bulk material can provide insights into their potential applications in optics, catalysis, catalysis, lithography, aerospace, thermal applications, and electronics. Overall, the present study can add physical insight into Mo–Be bonding, and enhance our understanding of these interactions in materials, offering valuable information for possible uses in the mentioned technologies.

4 Conclusions & final remarks

In the present study, we have explored the electronic structure and bonding of the ground and 42 low-lying states of the MoBe molecule, employing the (SA-)CASSCF and MRCISD(+Q) methodologies in conjunction with aug-cc-PV5Z(-PP) basis set. Bond distances, dissociation energies, dipole moments as well as common spectroscopic constants have been calculated while the bonding of selected calculated states is analyzed, and the variety of bonding schemes is further discussed.

The four lowest in energy states, $X^7\Sigma^+$, $a^5\Sigma^+$, $b^5\Pi$, $A^7\Pi$, are clearly separated from the remaining excited states in all used methods. The first excited state $a^5\Sigma^+$ is lying 15.0 kcal mol^{-1} above the ground one. Regarding the $X^7\Sigma^+$ state, it was found that a σ^1 dative bond is formed between the $4d_{z^2}$ single electron

of Mo and the vacant $2p_z$ orbital of Be with a length of 2.462 Å. The dissociation energy was calculated at 13.85 kcal mol^{-1} at the MRCISD+Q/aug-cc-pV5Z(-PP) method considering the correlation of the valence electron.

The adiabatic D_e values of calculated states, considering the correlation of all *ab initio* treated electron, range from 2.5 ($^9\Sigma^+(1)$) to 57.7 kcal mol^{-1} ($b^5\Pi$). Three states, namely $b^5\Pi$, $^3\Delta(1)$, and $^3\Pi(1)$ have triple bonds, and their diabatic D_e values, which are directly related to the bond strength, are 86.7, 92.0 and 88.0 kcal mol^{-1}. The calculated bond distances range from 2.047 Å, in $^3\Delta(1)$, up to 2.787 Å, in $^9\Sigma^+(1)$ while, the dipole moment values range from −1.51 D, in $X^7\Sigma^+$, "up" to 3.28 D, in $^9\Sigma^+(1)$.

The present work analyzes the bonding of the MoBe molecule. The Be atom participates actively in the formation of bonds by contributing its single valence electrons of its ground or first excited atomic state to Mo and/or passively become the recipient of electron density in its vacant orbitals, despite their high energy. The arising bonds vary from van der Waals interactions ($^9\Sigma^+(1)$), and half-bonds ($X^7\Sigma^+$), to triple bonds ($b^5\Pi$, $^3\Delta(1)$, and $^3\Pi(1)$). In most states, it is found a $2s2p_z$ hybridization on Be and a $4d_{z^2}5s5p_z$ hybridization on Mo, while electron charge is transferred from Be to Mo. As far as we know, the electronic spectrum of MoBe has never been studied before experimentally or theoretically. The binding schemes of all calculated states are presented for the first time filling the gap in the literature regarding diatomic molecules. It was found that on average, a single covalent Mo–Be bond is about 30 kcal mol^{-1}.

Overall, the present work highlights the exceptional ability of beryllium atoms to participate in a variety of bonding schemes, explaining experimental observations of chemically absorbed Be layers on Mo surfaces. Therefore, this study could provide an opening gate for further investigation of this species or associated material and complexes.

Conflicts of interest

There are no conflicts to declare.

Data availability

The data supporting this article have been included as part of the supplementary information (SI). Supplementary information: energetics of all MoBe calculated states at the CASSCF, SA-CASSCF, MRCISD, MRCISD+Q/aug-cc-pV5Z(-PP) methods and potential energy curves of the ground and excited states of MoBe at MRCISD level of theory. See DOI: **https://doi.org/10.1039/d5cp03025k**.

Acknowledgements

DT acknowledge computational time granted from the Greek Research & Technology Network (GRNET) in the National HPC facility ARIS under project ID pr015035-TrMeCo.

References

1 D. M. Dimiduk and J. H. Perepezko, *MRS Bull.*, 2003, **28**, 639–645.
2 A. Stevanovic, I. Cvijovic-Alagic and N. Mitrovic, *E3S Web Conf.*, 2024, **356**, 02016.
3 A. N. Shmelev, G. G. Kulikov, B. K. Kozhahmet, E. G. Kulikov and V. A. Apse, *Kerntechnik*, 2016, **81**, 596–598.
4 B. Cheng, P. Chou and Y.-J. Kim, *EPJ Nuclear Sci. Technol.*, 2016, **2**, 5.
5 G. Liu, G. J. Zhang, F. Jiang, X. D. Ding, Y. J. Sun, J. Sun and E. Ma, *Nat. Mater.*, 2013, **12**, 344–350.
6 P. Uranga, C. J. Shang, T. Senuma and H. Mohrbacher, *Adv. Manuf.*, 2020, **8**, 15–34.
7 S. G. Gordon, J. A. McGurty and G. E. Klein, *et al.*, *JOM*, 1951, **3**, 637–638.
8 C. R. Watts, *Trans. Metall. Soc. AIME*, 1969, **245**, 329–333.
9 A. S. Panov and M. M. Rysina, *J. Less-Common Met.*, 1977, **54**, 1–8.
10 T. Iwadachi, *US Pat.*, 6176418B1, 2001.
11 A. Eftekhari, *Appl. Surf. Sci.*, 2003, **220**, 343–348.
12 K. M. Skulina, C. S. Alford, R. M. Bionta, D. M. Makowiecki, E. M. Gullikson, R. Soufli, J. B. Kortright and J. H. Underwood, *Appl. Opt.*, 1995, **34**, 3727–3730.
13 S. Bajt, *J. Vac. Sci. Technol., A*, 2000, **18**, 557–559.
14 T. V. Afanasieva, A. G. Fedorus, A. G. Naumovets and D. V. Rumiantsev, *Surf. Sci.*, 2019, **682**, 14–24.
15 E. I. Stiefel and K. Othmer, *Encyclopedia of Chemical Technology*, Wiley, New York, 2001, p. 871.
16 J. F. Harrison, *Chem. Rev.*, 2000, **100**, 679–716.
17 D. Tzeli, I. Karapetsas, D. M. Merriles, J. C. Ewigleben and M. D. Morse, *J. Phys. Chem. A*, 2022, **126**, 1168–1181.
18 M. A. Mermigki, I. Karapetsas and D. Tzeli, *ChemPhysChem*, 2023, **24**, e202300365.
19 B. M. Hoffman, D. Lukoyanov, Z.-Y. Yang, D. R. Dean and L. C. Seefeldt, *Chem. Rev.*, 2014, **114**, 4041–4062.
20 M. V. White, E. E. Claveau, E. Miliordos and K. D. Vogiatzis, *J. Phys. Chem. A*, 2024, **128**, 2038–2048.
21 A. Androutsopoulos, D. Tzeli, K. H. Tomchak and M. D. Morse, *J. Chem. Phys.*, 2024, **160**, 234304.
22 T. Depastas, A. Androutsopoulos and D. Tzeli, *J. Chem. Phys.*, 2022, **157**, 054302.
23 L. Zhang, W. Zou, Y. Yu, D. Zhao, X. Maa and J. Yang, *J. Quant. Spectrosc. Radiat. Transfer*, 2021, **269**, 107690.
24 J. J. Sorensen, E. Tieu, A. Sevy, D. M. Merriles, C. Nielson, J. C. Ewigleben and M. D. Morse, *J. Chem. Phys.*, 2020, **153**, 074303.
25 C. Demetriou, C. E. Tzeliou, A. Androutsopoulos and D. Tzeli, *Molecules*, 2023, **28**, 8016.
26 J. M. Merritt, V. E. Bondybey and M. C. Heaven, *Science*, 2009, **324**, 1548–1551.
27 J. T. Boronski, A. E. Crumpton, L. L. Wales and S. Aldridge, *Science*, 2023, **380**, 1147–1149; J. Q. Nguyen, A. Rajabi, A. J. Wang, J. W. Ziller, F. Furche and W. J. Evans, *Organometallics*, 2023, **42**, 2185–2188.
28 G. Wang, J. E. Walley, D. A. Dickie, S. Pan, G. Frenking and R. J. Gilliard Jr., *J. Am. Chem. Soc.*, 2020, **142**, 4560–4564;

C. Berthold, J. Maurer, J. Langer, M. Morasch, S. Harder and G. Frenking, *Angew. Chem., Int. Ed.*, 2024, **63**, e202408422; M. A. Gosch, S. Pan, C. Poggel, N. Spang, M. Müller, G. Frenking and J. Sundermeyer, *Chem. – Eur. J.*, 2024, **30**, e202402118.

29 M. Lesiuk, M. Przybytek, J. G. Balcerzak, M. Musiał and R. Moszynski, *J. Chem. Phys.*, 2018, **148**, 224305; A. V. Mitin, A. A. Gusev, O. Chuluunbaatar, S. I. Vinitsky, V. L. Derbov and L. Le Hai, *J. Chem. Phys.*, 2023, **159**, 124307.

30 N. Fröhlich, U. Pidun, M. Stahl and G. Frenking, *Organometallics*, 1997, **16**, 528–537; M. Yáñez, P. Sanz, O. Mó, I. Alkorta and J. Elguero, *J. Chem. Theory Comput.*, 2009, **5**, 2763–2771.

31 K. Eskandari, *J. Mol. Model.*, 2012, **18**, 3481–3487; E. Fernández Villanueva, O. Mó and M. Yáñez, *Phys. Chem. Chem. Phys.*, 2014, **16**, 17531–17536.

32 K. Iversen, S. Couchman, D. Wilson and J. L. Dutton, *Coord. Chem. Rev.*, 2015, **297–298**, 40–48; M. E. Alikhani, *J. Mol. Model.*, 2020, **26**, 94.

33 J. Brandejs, L. Veis, S. Szalay, G. Barcza, J. Pittner and Ö. Legeza, *J. Chem. Theory Comput.*, 2023, **19**, 1112–1126.

34 L. Wang, S. Pan, G. Wang, X. Zeng, M. Zhou and G. Frenking, *Chem. Commun.*, 2022, **58**, 8532–8535; R. Liu, L. Qin, Z. Zhang, L. Zhao, F. Sagan, M. Mitoraj and G. Frenking, *Chem. Sci.*, 2023, **14**, 4872–4887; M. R. Buchner, S. Pan, C. Poggel, N. Spang, M. Müller, G. Frenking and J. Sundermeyer, *Chem. – Eur. J.*, 2024, **30**, e202400966.

35 D. Naglav, A. Neumann, D. Bläser, C. Wölper, R. Haack, G. Jansen and S. Schulz, *Chem. Commun.*, 2015, **51**, 3889–3891; G. Wang, J. E. Walley, D. A. Dickie, A. Molino, D. J. D. Wilson and R. J. Gilliard Jr., *Angew. Chem., Int. Ed.*, 2021, **60**, 9407–9411; C. Helling, D. J. D. Wilson and C. Jones, *J. Am. Chem. Soc.*, 2025, **147**, 16620–16629.

36 B. Jin, X.-L. Guan, M. Yan, Y.-J. Wang and Y.-B. Wu, *Chem. – Eur. J.*, 2023, **29**, e202302672.

37 X. Liu, M. Zhang, S. Yu, Y. Geng, X. Zhang, Y. Ding and Z. Su, *Phys. Chem. Chem. Phys.*, 2018, **20**, 23898–23902.

38 H. Rzepa, *Henry Rzepa's Blog*, 2022, DOI: **10.14469/hpc/10125**.

39 D. Tzeli and I. N. Karapetsas, *J. Phys. Chem. A*, 2020, **124**, 6667–6681.

40 D. Tzeli, *J. Comput. Chem.*, 2021, **42**, 1126–1137.

41 A. Rodriguez, S. Vadachkoria, F. A. Evangelista and M. C. Heaven, *J. Phys. Chem. A*, 2025, **129**, 2041–2048.

42 A. Androutsopoulos and D. Tzeli, *ACS Omega*, 2025, **10**, 40174–40189.

43 C. Demetriou and D. Tzeli, *Molecules*, 2025, **30**, 2874.

44 O. Roos, P. R. Taylor and P. E. M. Siegbahn, *Chem. Phys.*, 1980, **48**, 157–173.

45 H.-J. Werner and E. A. Reinsch, *J. Chem. Phys.*, 1982, **76**, 3144; P. J. Knowles and H.-J. Werner, *Chem. Phys. Lett.*, 1988, **145**, 514.

46 H.-J. Werner and P. J. Knowles, *J. Chem. Phys.*, 1988, **89**, 5803–5814.

47 K. A. Peterson, D. Figgen, M. Dolg and H. Stoll, *J. Chem. Phys.*, 2007, **126**, 124101.

48 B. P. Prascher, D. E. Woon, K. A. Peterson, T. H. Dunning Jr and A. K. Wilson, *Theor. Chem. Acc.*, 2011, **128**, 69–82.

49 M. Dolg, H. Stoll, H. Preuß and P. Schwerdtfeger, *Theor. Chem. Acc.*, 1997, **97**, 191–199.

50 H.-J. Werner and P. J. Knowles, *J. Chem. Phys.*, 1988, **89**, 5803.

51 S. R. Langhoff and E. R. Davidson, *Int. J. Quantum Chem.*, 1974, **8**, 61; M. R. A. Blomberg and P. E. M. Siegbahn, *J. Chem. Phys.*, 1983, **78**, 5682–5692.

52 J. L. Dunham, *Phys. Rev.*, 1932, **41**, 713.

53 R. S. Mulliken, *J. Chem. Phys.*, 1955, **23**, 1833–1840.

54 A. E. Reed, R. B. Weinstock and F. Weinhold, *J. Chem. Phys.*, 1985, **83**, 735–746; S. Ishikawa, G. Madjarova and T. Yamabe, *J. Phys. Chem. B*, 2001, **105**, 11986–11993; D. Tzeli, I. Petsalakis and G. Theodorakopoulos, *J. Phys. Chem. A*, 2011, **115**, 11749–11760.

55 P. J. Knowles, G. Knizia, F. R. Manby, M. Schütz, P. Celani, W. Györffy, D. Kats, T. Korona, R. Lindh *et al.*, MOLPRO 2015.1 is a package of *ab initio* programs written by H.-J. Werner.

56 F. Coester and H. Kiimmel, *Nucl. Phys.*, 1960, **17**, 477–485; K. Raghavachari, G. W. Trucks, J. A. Pople and M. Head-Gordon, *Chem. Phys. Lett.*, 1989, **157**, 479–483.

57 A. Kramida and W. C. Martin, *J. Phys. Chem. Ref. Data*, 1977, **26**, 1185–1194.

58 J. Sugar and A. Musgrove, *J. Phys. Chem. Ref. Data*, 1988, **17**, 155–239; A. Kramida, Y. Ralchenko, J. Reader, K. Olsen and R. Ibacache, *NIST Standard Reference Database 78, Version 5.12*, DOI: **10.18434/T4W30F**.

59 F. Biedermann and H.-J. Schneider, *Chem. Rev.*, 2016, **116**, 5216–5300.

